UNIVERSIDADE ESTADUAL DE CAMPINAS
Faculdade de Engenharia Mecânica

VICTOR ANTONIO SEIXAS DE MENEZES PAIVA

Static, Dynamic and Modal Analysis of Tensegrity Structures and Mechanisms

Análise Estática, Dinâmica e Modal de Estruturas e Mecanismos Tensegrity

CAMPINAS
2019

VICTOR ANTONIO SEIXAS DE MENEZES PAIVA

Static, Dynamic and Modal Analysis of Tensegrity Structures and Mechanisms

Análise Estática, Dinâmica e Modal de Estruturas e Mecanismos Tensegrity

Dissertation presented to the School of Mechanical Engineering of the University of Campinas in partial fulfillment of the requirements for the degree of Master in Mechanical Engineering, in the area of Mechanics of Solids and Mechanical Project.

Dissertação apresentada à Faculdade de Engenharia Mecânica da Universidade Estadual de Campinas como parte dos requisitos exigidos para a obtenção do título de Mestre em Engenharia Mecânica, na Área de Mecânica dos Sólidos e Projeto Mecânico. .

Orientador: Prof. Dr. Paulo Roberto Gardel Kurka

ESTE EXEMPLAR CORRESPONDE À VERSÃO FINAL DA DISSERTAÇÃO DEFENDIDA PELO ALUNO VICTOR ANTONIO SEIXAS DE MENEZES PAIVA, E ORIENTADA PELO PROF. DR. PAULO ROBERTO GARDEL KURKA.

.....
ASSINATURA DO ORIENTADOR

CAMPINAS
2019

Ficha catalográfica
Universidade Estadual de Campinas
Biblioteca da Área de Engenharia e Arquitetura
Luciana Pietrosanto Milla - CRB 8/8129

P166s

Paiva, Victor Antonio Seixas de Menezes, 1994-
Static, dynamic and modal analysis of tensegrity structures and mechanisms / Victor Antonio Seixas de Menezes Paiva. – Campinas, SP : [s.n.], 2019.

Orientador: Paulo Roberto Gardel Kurka.
Dissertação (mestrado) – Universidade Estadual de Campinas, Faculdade de Engenharia Mecânica.

1. Dinâmica. 2. Estática. 3. Método elementos finitos. 4. Vibrações. 5. Cinemática. I. Kurka, Paulo Roberto Gardel, 1958-. II. Universidade Estadual de Campinas. Faculdade de Engenharia Mecânica. III. Título.

Informações para Biblioteca Digital

Título em outro idioma: Análise estática, dinâmica e modal de estruturas e mecanismos tensegrity
Palavras-chave em inglês:
Finite element method
Kinematics
Flexible structures
Modal analysis
Cable structures
Área de concentração: Mecânica dos Sólidos e Projeto Mecânico
Titulação: Mestre em Engenharia Mecânica
Banca examinadora:
Paulo Roberto Gardel Kurka [Orientador]
Niederauer Mastelari
Jaime Hideo Izuka
Data de defesa: 31-07-2019
Programa de Pós-Graduação: Engenharia Mecânica

Identificação e informações acadêmicas do(a) aluno(a)
- ORCID do autor: https://orcid.org/0000-0003-2862-1717
- Currículo Lattes do autor: http://lattes.cnpq.br/7439457585525706

Agência(s): CNPq
Nº do Proc.: 132166/2018-6

UNIVERSIDADE ESTADUAL DE CAMPINAS
FACULDADE DE ENGENHARIA MECÂNICA
COMISSÃO DE PÓS-GRADUAÇÃO EM ENGENHARIA MECÂNICA

DEPARTAMENTO DE SISTEMAS INTEGRADOS

DISSERTAÇÃO DE MESTRADO ACADÊMICO

Static, Dynamic and Modal Analysis of Tensegrity Structures and Mechanisms

Análise Estática, Dinâmica e Modal de Estruturas e Mecanismos Tensegrity

Autor: Victor Antonio Seixas de Menezes Paiva

Orientador: Prof. Dr. Paulo Roberto Gardel Kurka

A Banca Examinadora composta pelos membros abaixo aprovou esta Dissertação:

Prof. Dr. Paulo Roberto Gardel Kurka
Faculdade de Engenharia Mecânica - UNICAMP

Prof. Dr. Niederauer Mastelari
Faculdade de Engenharia Mecânica - UNICAMP

Prof. Dr. Jaime Hideo Izuka
Faculdade de Ciências Aplicadas - UNICAMP

A Ata da defesa com as respectivas assinaturas dos membros encontra-se no processo de vida acadêmica do aluno.

Campinas, 31 de julho de 2019.

Dedicatória

Dedico este trabalho aos meus pais Maria Lucia e Antonio, à minha avó Umbelina e às memórias dos meus avós Manuel, Antonio e Felícia.

Agradecimentos

O presente trabalho foi realizado com apoio do CNPq, Conselho Nacional de Desenvolvimento Científico e Tecnológico – Brasil. Processo 132166/2018-6.

Ao meu orientador prof. Dr. Paulo Kurka pela oportunidade e pelos desafios oferecidos.

Ao professor Dr. Jaime Izuka pela paciência, pelas sugestões, por indicar *tensegrity* como tema e por fazer inúmeras viagens de Limeira a Campinas para acompanhar o trabalho.

Aos meus amigos de laboratório Luis, Renato e Paola, por me ajudarem com os protótipos, experimentos e códigos e ao Matheus Carioca e Pedrinho pelo convívio e amizade.

Aos professores Dr. Niederauer Mastelari e Dr. Caio Santos pelas correções e contribuições feitas no texto final.

Aos meus amigos Breno, Okida, Baldasso (pela disciplina), Gabriel, Raphael, Andre, Lucas, Minoru e Serginho pelo companheirismo.

Ao pessoal das caronas de São Paulo a Campinas, por tornarem minhas noites de domingo mais felizes e os quilômetros mais curtos.

À minha família, incluindo minha namorada Andréia e sua mãe Akemi, pelo apoio psicológico, que foi fundamental neste período, e pela hospitalidade.

Resumo

O desenvolvimento de estruturas mais leves, finas, rígidas ou inteligentes é um desafio constante entre engenheiros e cientistas de qualquer área. Sistemas *tensegrity*, que são formados por corpos rígidos em compressão e cabos em tração, têm perspectiva de serem amplamente aplicados pelas indústrias espacial, civil, mecânica, aeronáutica ou biomédica. O projetista de um *tensegrity* pode controlar sua rigidez e formato através da mudança de tensão nos cabos, cujos comportamentos são explorados neste trabalho via protótipos e simulações. Um modelo foi sugerido para otimizar massa e volume de uma antena de satélite, o mecanismo *tensegrity* foi criado para ser lançado num formato colapsado, economizando volume dentro do foguete, e expandido no espaço através da contração de determinados cabos. Em seguida, as tensões dos cabos de um prisma *tensegrity* foram variadas e a mudança na rigidez foi avaliada por análise modal. Por fim, uma torre *tensegrity* bidimensional foi submetida a grandes deformações, sua análise estática não linear foi implementada e as frequências naturais das posições deformadas foram calculadas. As três metodologias foram implementadas e, posteriormente, validadas em três experimentos distintos, estes ressaltando os efeitos de cada propriedade em avaliação. O objetivo deste trabalho é propor um procedimento para desenvolver o projeto e construção de uma estrutura *tensegrity* que englobe as três metodologias: definindo sua expansão a partir de uma configuração colapsada, o controle da rigidez quando estável e a nova posição caso algum esforço provoque grandes deformações. Portanto, além do objetivo prático do primeiro tópico, este trabalho tem como meta fornecer uma documentação geral de soluções relacionadas a estruturas e mecanismos *tensegrity*.

Palavras-chave: *tensegrity; estruturas; dinâmica*.

Abstract

The development of lighter, thinner, stiffer or smarter structures is a constant challenge among engineers and scientists of all fields. Tensegrity systems, which are formed by rigid bodies under compression and cables under traction, are likely to be largely used by the space, civil, mechanical, aeronautical and biomedical industries. The designer of a tensegrity can control its stiffness and shape by changing the tension in the cables, these behaviours are explored in this work via prototypes and simulations. A model was suggested to optimize mass and volume of a satellite antenna, a tensegrity mechanism was created to be launched in a reduced shape, saving volume in the launcher, and expanded in space by pulling specific tendons. Secondly, the tensions of a tensegrity prism's cables were varied and the change in stiffness was assessed through modal analysis. Finally, a 2D tensegrity tower was put under large deformations, its nonlinear static analysis was implemented and the natural frequencies of the deformed configurations were calculated. All the three methodologies have been implemented and, later, validated through experiments designed to highlight each property of concern. The objective of this work is to propose procedures to develop and build a tensegrity structure that carry those three methodologies: defining its expansion from a compact configuration, its stiffness control once the expansion is finished and its new shape if any load generates large displacements. Thus, beyond the practical end of the first topic, the goal of this work is to provide a general document of solutions related to tensegrity structures and mechanisms.

Keywords: *tensegrity; structures; dynamics*.

List of Figures

List of Tables

List of Abbreviations and Symbols

v – Length of the inclined cable.

ψ – Twist angle.

h – Height.

l – Dimension of the base.

N – Nodes matrix.

b – Length of a strut.

E_P – Potential energy.

E_F – Energy dissipated by friction.

E_E – Energy of the engine.

F_F – Friction force.

F_E – Force of the engine.

m – Mass of a bar.

g – Gravity.

$\dot{W}$ – Engine power.

W – Weight.

t – Time.

F_X – Forces about axis X.

F_Y – Forces about axis Y.

F_Z – Forces about axis Z.

E – Young Modulus.

A – Cross-section area.

L – Length.

σ – Stress.

s – Force density.

n_i – Node coordinates.

n – Total number of nodes.

m – Total number of members.

C – Connectivity matrix.

c – Connectivity vector.

e_i – Vetical vector full of zeros with 1 in the i^{th} position.

e_j – Vertical vector full of zeros with *1* in the j^{th} position.

K_B – Stiffness of a bar.

I – Identity matrix.

φ – Shape function.

le – Length of the element.

ρ – Density.

M – Members matrix.

ω – Natural frequencies.

$\{d\}$ – Vibration modes.

H – Mass matrix.

K – Stiffness matrix.

n_s – Number of struts.

ψ_s – Stable twist angle.

τ_B – Pre-tension in the bar.

τ_H – Pre-tension in the horizontal cable.

τ_V – Pre-tension in the inclined cable.

τ_E – Extra traction.

L_T – Total length.

E – Young modulus.

P – Force acquired by the scale.

Θ – Angle in the tensiometer scheme.

T – Traction.

a – Dimension in the tensiometer scheme.

b – Dimension in the tensiometer scheme.

$\{x\}$ – Displacements vector.

$\{F\}$ – Loads vector.

p – Number of steps.

ε – Elongation.

H – Matrix used in the definition of the Kronecker product.

G – Matrix used in the definition of the Kronecker product.

α – Number of lines in G.

β – Number of columns in G.

i – Number of lines in H.

j – Number of columns in H.

Subscripts

i – i^{th} node.

k – k^{th} element.

G – Global.

Contents

1 INTRODUCTION

The term “tensegrity” is considerably recent, it was suggested by Fuller (1975), combining the words “tension” and “integrity”. Despite having created the name, the history of the invention itself is cloudy and can be shared with Kenneth Snelson and David Georges Emmerich. Furthermore, in 1920 Karl Ioganson patented a structure with three bars and eight cables, which may be seen as a first step for the other inventors’ configurations (JAUREGUI, 2009).

Briefly, a tensegrity is formed by compressed rigid bodies suspended by a continuous network of cables under pure tension (PUGH, 1976). A tensegrity configuration is an unstable set of rigid bodies that can be stabilized by a combination of cables, without external forces. After connecting a tensegrity configuration to the referred combination of cables, it may be called a tensegrity system (SKELTON and DE OLIVEIRA, 2009). The class of a tensegrity is given by the maximum number of rigid bodies in contact, and the class is 1 if the rigid bodies do not touch. Snelson’s needle tower (Figure 1) is an example of a class 1 tensegrity.

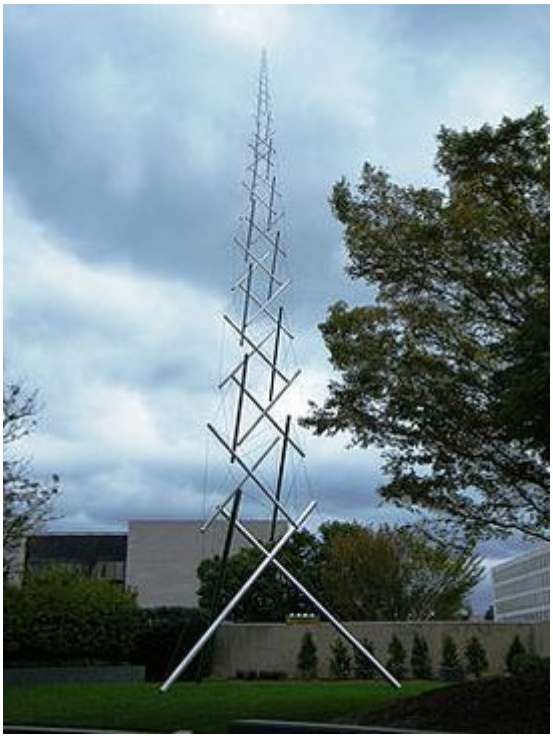

Figure 1. Needle tower.

The elements of a tensegrity system are designed to stress in only one direction each, cables must be under traction and bars under compression (ASHWEAR and ERIKSSON, 2014), which allows a more efficient material selection and simplifies the equations. Simpler equations lead to precise models and a better material selection leads to a higher structural efficiency. Both benefits are important for a number of fields in engineering, for example, aerospace engineers always seek lighter structures and accurate simulations, as they have limited payload and any miscalculation can be extremely expensive. These advantages are convenient for civil engineering applications too, the Kurilpa bridge (Figure 2) is an example of a hybrid tensegrity structure.

Figure 2. Kurilpa bridge in Brisbane, Australia.

A third advantage of tensegrities is the ability to change its shape and stiffness by changing the pre-stresses in the cables. By proportionally changing the tension of all tendons, the shape will keep and the stiffness will change, but by asymmetrically varying the tension, the shape will transform. Additionally, regarding control, traditional beams and trusses are forced to show an unnatural behaviour when actuated, while a tensegrity can have its equilibrium changed. In other words, the designer can change the nature of the system instead of forcing against a fixed equilibrium, as done nowadays with traditional structures. An illustration of this application is the rolling system of the Demoiselle (Figure 3), a cable connects the tip of the wing and the bottom of the fuselage, once pulled, the wing changes its shape and therefore its lift, making the airplane roll, performing the function of ailerons in later airplanes.

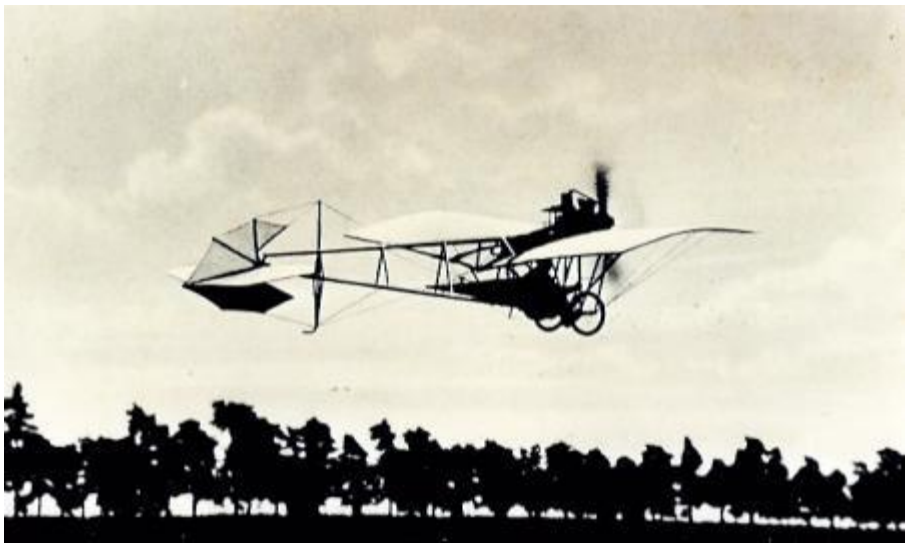

Figure 3. Santos Dumont's Demoiselle.

This work contains three main topics: the expansion of a deployable tensegrity, modal analysis of a tensegrity prism with variable pre-stress and a nonlinear static analysis on a 2D tensegrity tower. Three prototypes were built so the models could be validated, one for each study: prototype 1 reduces or expands by relaxing or pulling the cable (Figure 4), prototype 2 can be tensioned or relaxed according to the torque applied on the screws (Figure 5) and prototype 3 is subjected to large deformations (Figure 6).

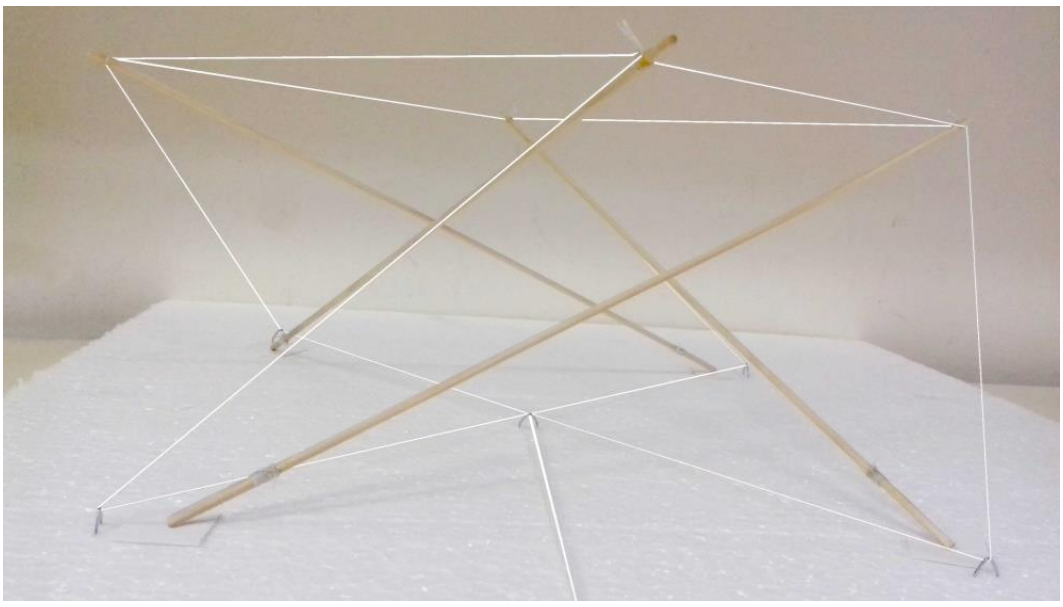

Figure 4. Prototype 1.

Figure 5. Prototype 2.

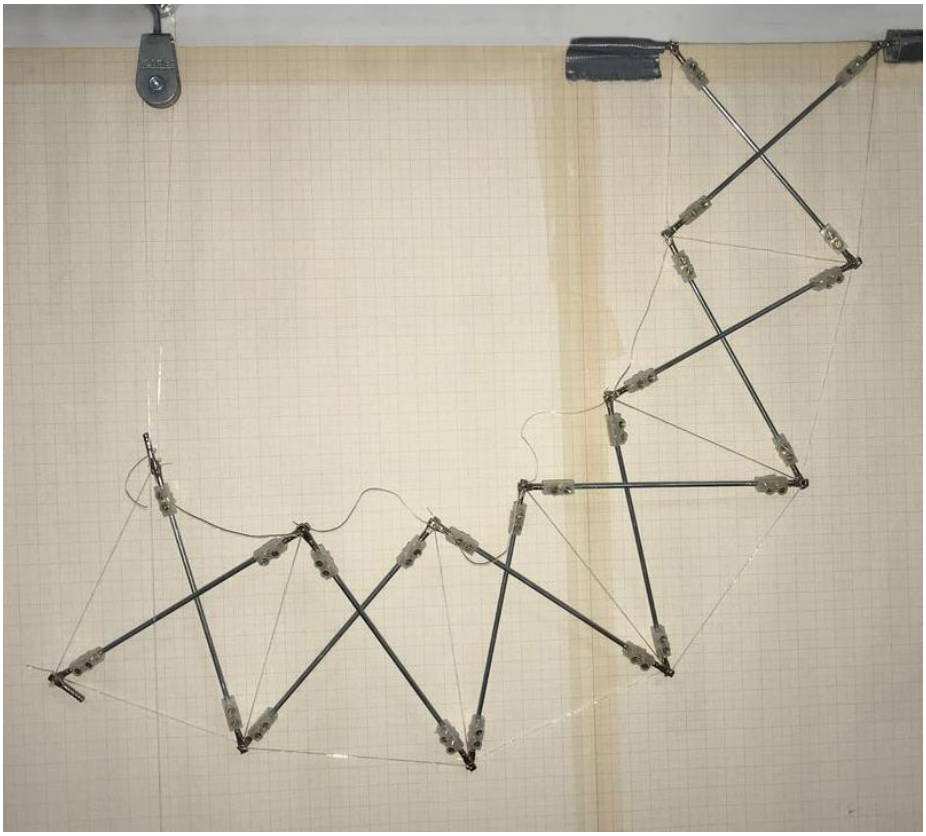

Figure 6. Prototype 3.

The first model was created to support the reflector antenna of a satellite so the mechanism could be launched in its compacted shape, saving volume in the launcher, and expanded only in space. The second prototype does not have an immediate application, but

the phenomenon has, and that configuration was chosen to simplify its assessment. The last prototype is a possible manipulator, as the position and angle of the tip nodes change with the loads, this tensegrity could perform the functions of light robotic arms or mobile camera stands in space missions, for example.

1.1 Objectives

Each model has an individual application and highlights a different tensegrity characteristic, so the specific objectives of this work consist in:

- Developing a tensegrity mechanism and defining its kinematics and dynamics.
- Calculating the stiffness of a tensegrity and assessing its sensitivity to the pre-stresses.
- Solving the nonlinear static analysis of a long and flexible tensegrity tower.
- Validating the methodologies with experiments.

The general goal of this study, however, is to document an introductory guide (Figure 7) on structural and dynamic analyses of tensegrities, by combining the methodologies described in this work.

For example, starting from a compact shape, the kinematic analysis is performed to define the transformation into the expanded form. Once fully deployed, the mechanism becomes a static structure. Then, given an external load, a static analysis is required to calculate the final shape and internal stresses of the tensegrity. If the loads are relatively small, the linear analysis based on Skelton's work is applied, otherwise Euler's method is combined to solve the nonlinear analysis. Finally, the stiffness of the structure can be controlled through stressing or relaxing the tendons.

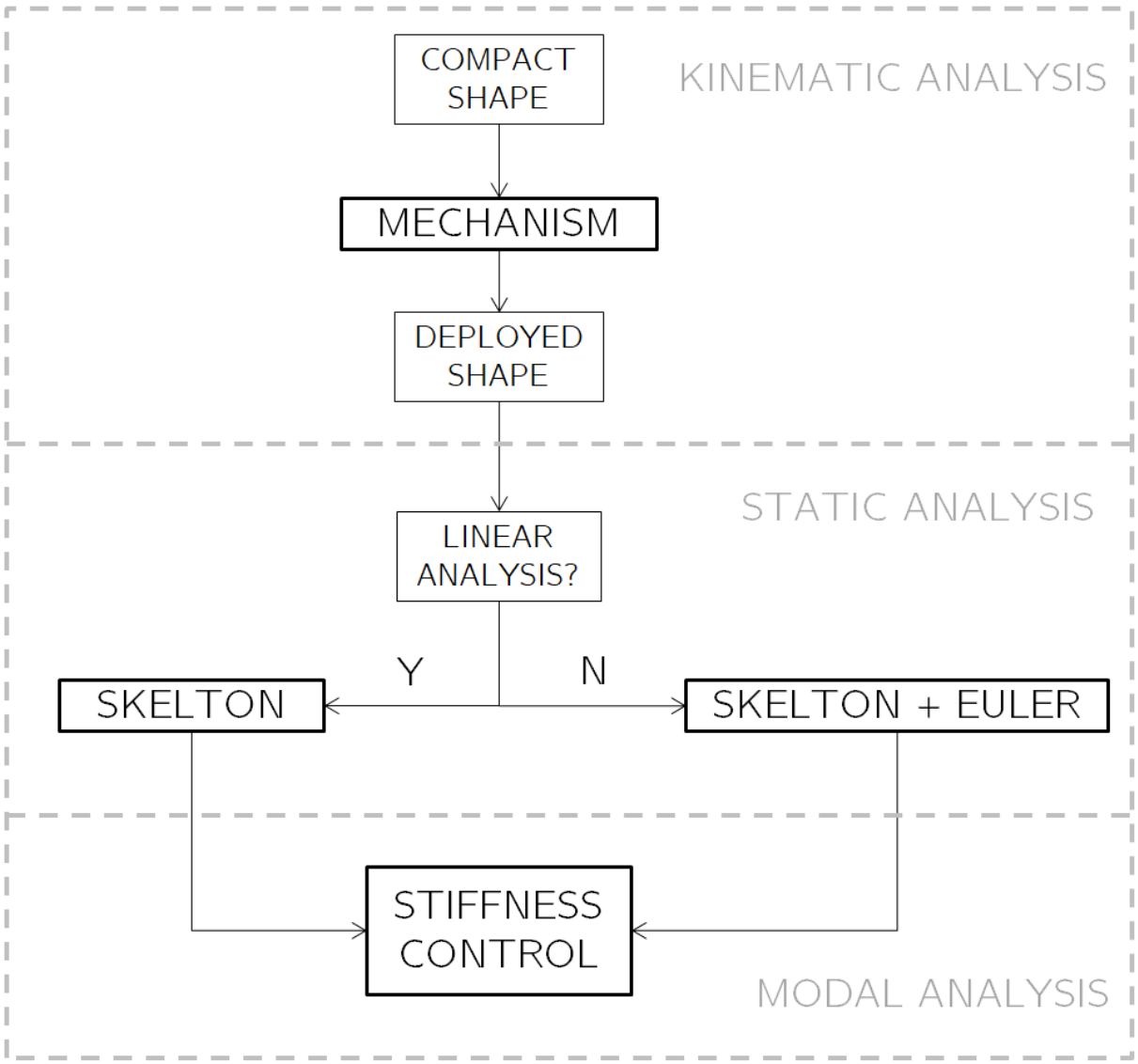

Figure 7. Guide.

1.2 Dissertation Structure

Chapter 2 reviews the literature about tensegrities in general and then focuses on each model studied in this work. Chapters 3, 4 and 5 relate to prototypes 1, 2 and 3 respectively, detailing the numerical and experimental methodologies, highlighting their specific characteristics and showing the comparison between practical and mathematical results. Finally, chapter 6 shows the main conclusions, limitations of the procedures, future steps and supports the importance of studying tensegrity structures and mechanisms.

2 LITERATURE REVIEW

Tensegrity systems have a high interdisciplinary potential. Friesen (2016) suggested and prototyped a tensegrity robot to climb ducts, its features are advantageous to dodge obstacles and overcome corners and diameter variations in a pipe. Jensen (2007) proposed the use of tensegrity beams for aquaculture installations and simulated them using a finite element software. Health professionals have also seen usefulness related to tensegrities, either by suggesting innovative prostheses (JUNG, LY, *et al.*, 2019) and simulating parts of the body, such as a spine (LEVIN, 2002). Biologists have replicated animals' features (FRANTSEVICH and GORB, 2002) and modelled the mechanical behaviour of living cells (INGBER, 1997) and (WANG, SRBOLJUB, *et al.*, 2001).

In the field of civil engineering, the use of tensegrity structures in roofs, domes and towers (GILEWSKI, KLOSOWSKA and OBARA, 2015) can be simply justified by their high structural efficiency, but the ability to deploy has been essential for some projects. For example, the retractile bridge for pedestrians of Rhode-Barbarigos (2010) do not limit the height of vehicles of the road. Also, structures that adapt their shape or stiffness, instead of remaining static and passive, are attractive to civil engineers because the external loads (or constraints) may not be always constant, and tensegrities have this adaptive property (ADAM and SMITH, 2008).

In aerospace engineering, however, the deployment capacity brings even greater advantages, such as the possibility of sending a compressed structure to space to be expanded only on orbit, saving volume inside the launcher. A growing demand on larger reflector antennas supports the application of tensegrity systems in space structures (ZHANG and OHSAKI, 2015). A tensegrity-membrane antenna called Astromesh (THOMSOM, 1999) had its dynamic behaviour studied and verified through a prototype by Moterolle (2015). Analogously, a hexagonal prism designed to perform the same purpose was analysed by Fazli (2011) in terms of dynamics and by Kurka (2018) in terms of deployment. Teixeira (2018) verified the impact of the membrane on the stiffness of the system, which performs the function of a reflector surface or an energy harvesting mechanism (SUNNY, SULTAN and KAPANIA, 2014).

This work contains three main topics which are addressed by sections **2.1 Expansion of retractile structures and deployable tensegrities, 2.2 Stiffness Control** and **2.3 Long and flexible structures**. These three topics are related but were studied separately to better highlight each property: deployment, controlling stiffness through pre-stressing and large deformations taking the pre-stresses into account. Retractile structures were not explored in this work but were considered in the literature review because they may have the same applications as deployable tensegrities.

2.1 Expansion of retractile structures and deployable tensegrities

A literature review of retractile structures, concerning space applications, is relevant to analyse the existing alternatives and indicate their limitations (PELLEGRINO, 2001) and (TIBERT, 2002). Just as tensegrities, retractile structures may transform their shape from a compact to an expanded configuration, reaching longer lengths. During launch, retractile structures can sustain the loads in the compact shape, which saves mass considering how heavier the structure would be if the loads had to be sustained by the geometry of the expanded shape. The small size of the compact form and the precision of the expanded shape give the retractile structures a high cost-performance ratio.

Tubular retractile structures of thin wall made of steel, copper-beryllium alloys or polymers strengthened with carbon fibre were pioneer in the space industry, taking advantage of the elastic behaviour of these materials. STEM (storable tubular extendible member) and CMT (collapsible tubular mast) are the two main kinds. Telescopic structures are concentric cylinders stored inside of each other, largely used as camera stands in transmission vehicles or mobile watch towers.

Retractile trusses were developed to help with the problems associated to storing and attaching big space structures during launch. Zhang (2014) built retractile trusses of high reliability with glass fibre composites and shape memory polymers. These articulated bar structures appear in numerous configurations and a few eventually converge into something similar to a tensegrity system, such as the cable strengthened pantograph. In other words,

retractile structures are proper for space applications because they deploy, but tensegrities might be one step further in terms of lightness and accuracy.

There are numerous possibilities concerning the expansion of a tensegrity structure. Pellegrino (2001) suggested varying the length of a cable or strut and calculating by geometry the new nodes positions. Arsenault and Gosselin (2009) replaced six tendons of a prism by springs, added actuators to the bars so their length could be changed and used the Jacobian matrix to calculate the kinematics of the structure analytically.

Russel and Tibert (2008) replaced the elements under traction by inflatable films, so the system could be deployed by filling them with air. The kinematic analysis was performed by LS-DYNA with a finite element model created in Ansys. Zolesi (2012) simulated the expansion of a *12m* diameter deployable antenna through a numerical model and commented about the form-finding property. A similar structure had its expansion process analysed by Rhode-Barbarigos (2012), but through a variation of the dynamic relaxation method.

As described and used by Bel Hadj Ali (2011), this method of dynamic relaxation applies fictitious masses and damping in the equations of motion, making the static problem become dynamic, and solves the motion equations as a function of time through finite differences. The nodes positions are calculated every instant and the fictitious damping leads them to rest statically in the end. The properties of the strings (or the power of the actuators) required to activate the expansion can be calculated by the energy method used by Bel Hadj Ali and described by Moored (2009).

Given the pre-stresses of a tensegrity, the designer may find its respective shape through a form-finding method (ZHANG and OHSAKI, 2015), this feature can be useful for the expansion analysis and for the stiffness control. The force density algorithm departs from an initial guess for the set of pre-stresses, calculates its closest feasible set of pre-tensions given the geometry of the structure and finally finds the nodes positions for that calculated set of pre-tensions.

Schenk (2006) placed a tensegrity prism prototype in many static and symmetric positions by varying the lengths of its members. In this study, a similar system was developed, but the contribution relies in producing a continuous movement. The contraction of a determined set of cables enables this steady transformation, which also allows the movement to happen in a physical model. Its kinematics was calculated by geometry and the prototype was analysed through image processing by tracking the interesting spots of the

structure, analogous to what Lessard (2016) and Baltaxe-Admony (2016) designed for their works in biomechanics.

Yang (2019) suggested a foldable tensegrity-membrane system, which unfolds the membrane during the deployment process. In this work, the compact shape of the proposed mechanism may occupy a larger area, but the membrane could be attached to its top base, perform the function of the reflector surface and would not have to fold or unfold anytime.

Additionally, the deployable characteristic of tensegrities can also be used to produce walking robots (PAUL, VALERO-CUEVAS and LIPSON, 2006) and (SUNSPIRAL, AGOGINO and ATKINSON, 2015). Tensegrity robots for space exploration withstand impact loads better than regular probes, so when it comes to landing, structural efficiency and deployment, tensegrities are preferred.

High structural efficiency and controllable stiffness are essential advantages of tensegrities, but may not be enough to motivate engineers to move from their comfort zone: traditional and established beams or trusses. On the other hand, the possibility of deployment turns the table regarding the range of applications, and tensegrities may be massively used once this ability becomes well established. Documenting experiments and producing research material are necessary steps for making tensegrities reliable, this work aims to support achieving this objective.

2.2 Stiffness Control

One of the main advantages of tensegrities is the possibility to change the stiffness by varying the pre-stresses of the cables. Furuya (1992) was probably the first to verify the stiffness control through modal analysis of a tensegrity tower, confirming that the natural frequencies increase with the pre-stresses. Bel Hadj Ali (2010) converged to the same conclusion more recently, but combining experiments and simulations. Working with different excitation frequencies, they managed to alter the pre-stress so the natural frequency of the structure avoided the excitation’s, controlling the amplitudes of vibration. Finally, Yang and Sultan (2016) sequenced the deployment of a tensegrity-membrane system and modelled a control strategy.

With simulations and physical experiments on a 9 cables and 3 bars tensegrity, Motro (1986) showed that the nonlinear behaviour of simple structures can be reasonably approximated by a linear model. However, Yang and Sultan (2014) concluded from a 4 bars and 4 cables membrane-tensegrity that a linear elastic model is not accurate when the displacements of the membrane are large enough.

The stiffness of a cable depends on its pre-stress and geometrical orientation, which is given by the shape of the tensegrity. The shape can be found through a form-finding method, and its inputs include the pre-stresses of the cables as well (PAGITZ and TUR, 2009) and (ZHANG and OHSAKI, 2006). Therefore, controlling the global stiffness of the structure through pre-stressing requires attention as it may affect the geometry. Furthermore, the pre-stresses can be used to redesign the geometry so the structure shows a greater stiffness in a certain direction, not only because the members are more stressed but also because their orientations contribute (SKELTON, ADHIKARI, *et al.*, 2001).

This work contains a stiffness study, similar to Furuya's (1992), but with a 3D tensegrity prism. The contribution lies in validating a methodology based on Skelton's work (which calculates stiffness given the pre-stresses) with a prototype, using an image processing software to acquire the natural frequencies. Despite not having much impact in terms of innovation, this step is vital for serving as basis to the development of the next model. A future work could involve adding actuators to the prototype and implementing an active control methodology (DJOUADI, MOTRO, *et al.*, 1998).

2.3 Long and flexible structures

Manipulators and robotic arms usually need to be precise and engineers end up having to design them stiff and heavy to guarantee their accuracy. Heavy mechanisms lead to slow movements or extremely powerful and expensive engines. However, regardless of the price, heavy structures are not suitable for space applications, challenging the community to design light and accurate manipulators.

Holland (2008) studied large deflections and vibrations of a long beam to support its application on solar sails, whose highly flexible booms may buckle. A long and flexible beam

with a camera attached to its tip was suggested by Kurka (2016) to acquire images from the top of an outdoor exploration vehicle. It is interesting to keep the probe as high as possible to reach a farther horizon, the vibrations are H_∞ controlled by an actuator cable that connects the tip of the beam to the base. Furthermore, when the vehicle comes to terrain slopes, the beam can bend (pulled by the cable) and move the camera to acquire images from different positions and inclinations (KURKA, IZUKA, *et al.*, 2014). In this work, a 2D tensegrity tower (Figure 6) replaces the beam, therefore combining the advantages of tensegrities with the applications considered for the long and flexible beam. Feng (2018) modelled a tensegrity beam and applied an active control technique to mitigate its vibration, but seems to lack experimental results, designing a similar control technique to the proposed 2D tower or a prototype to Feng's model can be a future step.

Kebiche (1999) modelled a tensegrity beam made of several 4 struts prisms in sequence and analysed its geometrical nonlinearities. Dalilsafaei (2012) also modelled a tensegrity boom, but with 3 struts prisms instead, and attempted to improve its bending stiffness. Moored (2007) designed a tensegrity beam as well, but with morphing abilities, in three dimensions and without a prototype. Its shape shifting condition was initially proposed to control the core of a morphing wing and imitate a manta ray, but it can be easily adapted to work as a camera stand in a space probe as well.

Skelton's method for tensegrities cannot be directly applied to this case because the displacements are too large, making the static analysis nonlinear, so the contribution of this study relies in combining the incremental loads (or Euler's) method (CRISFIELD, 2000) for nonlinear finite element analysis with Skelton's method for tensegrity structures. Struts that are not perfectly straight lead to a nonlinear behaviour when compressed (CAI, YANG, *et al.*, 2019). The buckling effect creates this nonlinearity and was studied by Ashwear (2014), who used beam (instead of bar) elements to model the struts and therefore managed to analyse their resistance to bending.

Zhang (2013) also used increments for solving static analyses of tensegrities, but combined with a self-adaptive methodology to increase the robustness of the method as a whole. Tran (2011) developed a similar study, but instead of the incremental loads method for nonlinearities, they used both total and updated Lagrangian formulations to establish the equations and a variation of Newton-Raphson's method to solve them, similar to Murakami's (2001) work. Their model had a high number of elements, making those more complex methods convenient, however, in this work, the 2D tower under analysis contains a small

number of elements, minimizing the impact of Euler's method's lower efficiency and highlighting its simplicity.

Kan (2018) designed a tensegrity framework, studied its movement and highlighted the roughness generated by cables that keep switching between slack and taut states. In this study, these transitions create discontinuities in the natural frequencies from one static position to the other. Therefore, the tendons should be pre-stressed before the analysis to postpone the occurrence of slack cables.

The trade-off involving length, lightness, stiffness and accuracy challenges the designers of a long and flexible structures since high aspect ratio and low stiffness bring a low accuracy that is not convenient. Therefore, tensegrity structures can be helpful in this context, since they are highly mass efficient and their stiffness and shape can be controlled by the stresses of their cables, which inspires the analysis of a flexible tensegrity tower in this work.

3 KINEMATICS OF A TENSEGRITY IN EXPANSION

The reflector surface of a satellite antenna is supported by a stiff cone that keeps it on a minimum distance from the wall of the satellite (Figure 8). This distance is necessary because the part of the signal that misses the surface could reflect on the wall of the satellite and come to Earth generating noise. The diameter of this antenna is around *0.5 m* and the stand is approximately *0.2 m* tall.

The aim of this chapter is to develop a tensegrity system to replace these stiff and heavy stands of reflector antennas. Such system must be deployable, so the structure can be sent to space in its compact form, saving volume in the rocket, and expanded only on orbit, where volume ceases to be an issue. Furthermore, the stiffness of a tensegrity can be controlled by the stresses in the cables, which adds one more feature in favour of this innovative design.

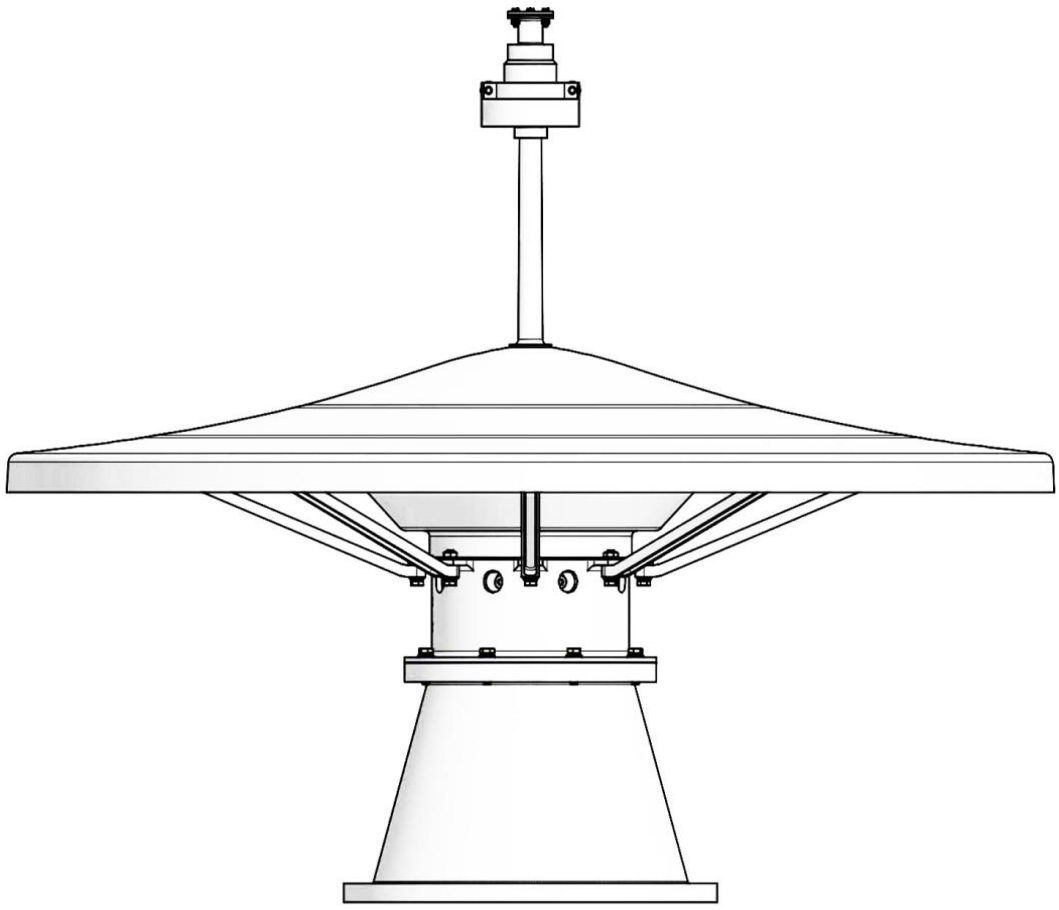

Figure 8. Antenna.

Another possibility of this system is to exchange the reflector surface, which is metallic, by a lighter membrane made of a reflective material, turning it into a tensegrity-membrane system (KURKA, PAIVA, *et al.*, 2018), but the objectives of this work focus on the dynamics of the expansion process of the tensegrity part.

3.1 Description of the system

The system to be studied is a four struts tensegrity prism (Figure 9). The lower base is fixed to the ground and the upper base moves up and down, but its plane remains always parallel to the ground. Such movement is driven by the cables that connect the two bases, they change length at the same rate, keeping the bases parallel and the system symmetric. The other tendons and struts are constant in length.

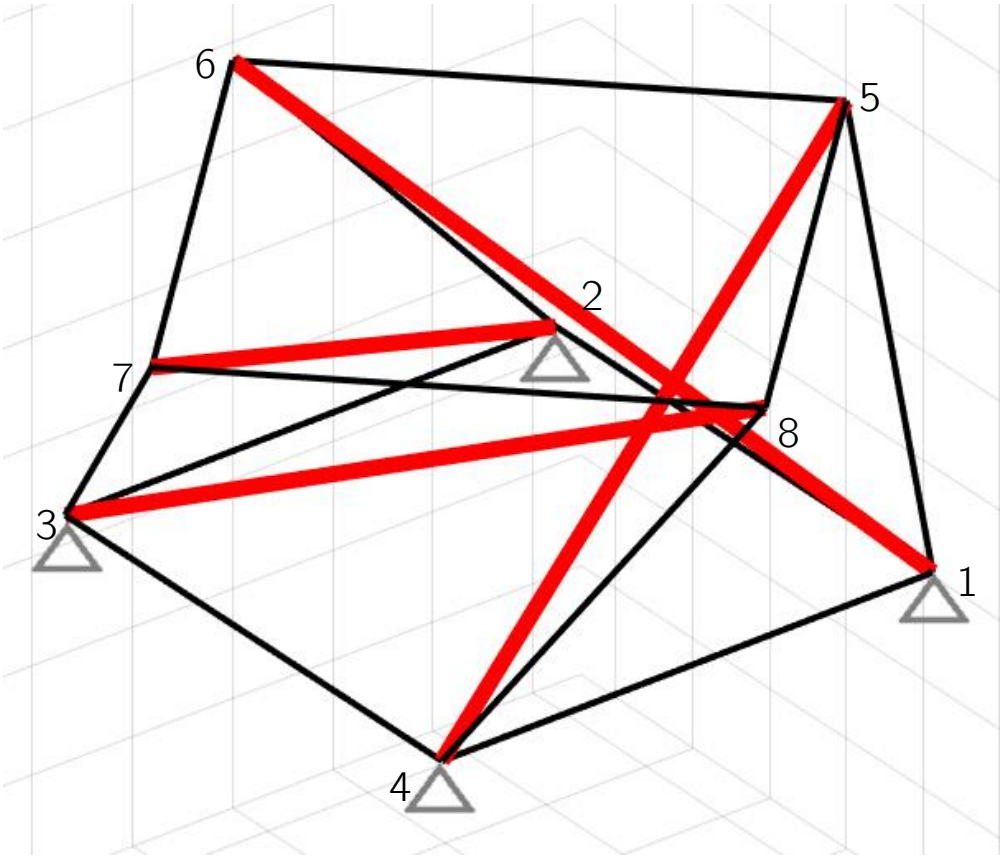

Figure 9. 4 struts tensegrity prism. (PAIVA, KURKA and IZUKA, 2018)

3.2 Geometry

The lower nodes are fixed, so the shape of this system is defined by the upper nodes positions. As the length *v* of the inclined cables is varied, the twist angle ψ and the height *h* of the structure change, the length *b* of the bars and the side *l* of the bases are constant.

Applying loop equations (DOUGHTY, 1988) on the top view (Figure 10). The nodes matrix *N* containing the positions of the *8* nodes can be determined, the cosine and sine of the twist angle ψ were simplified with the notations *c* and *s*.

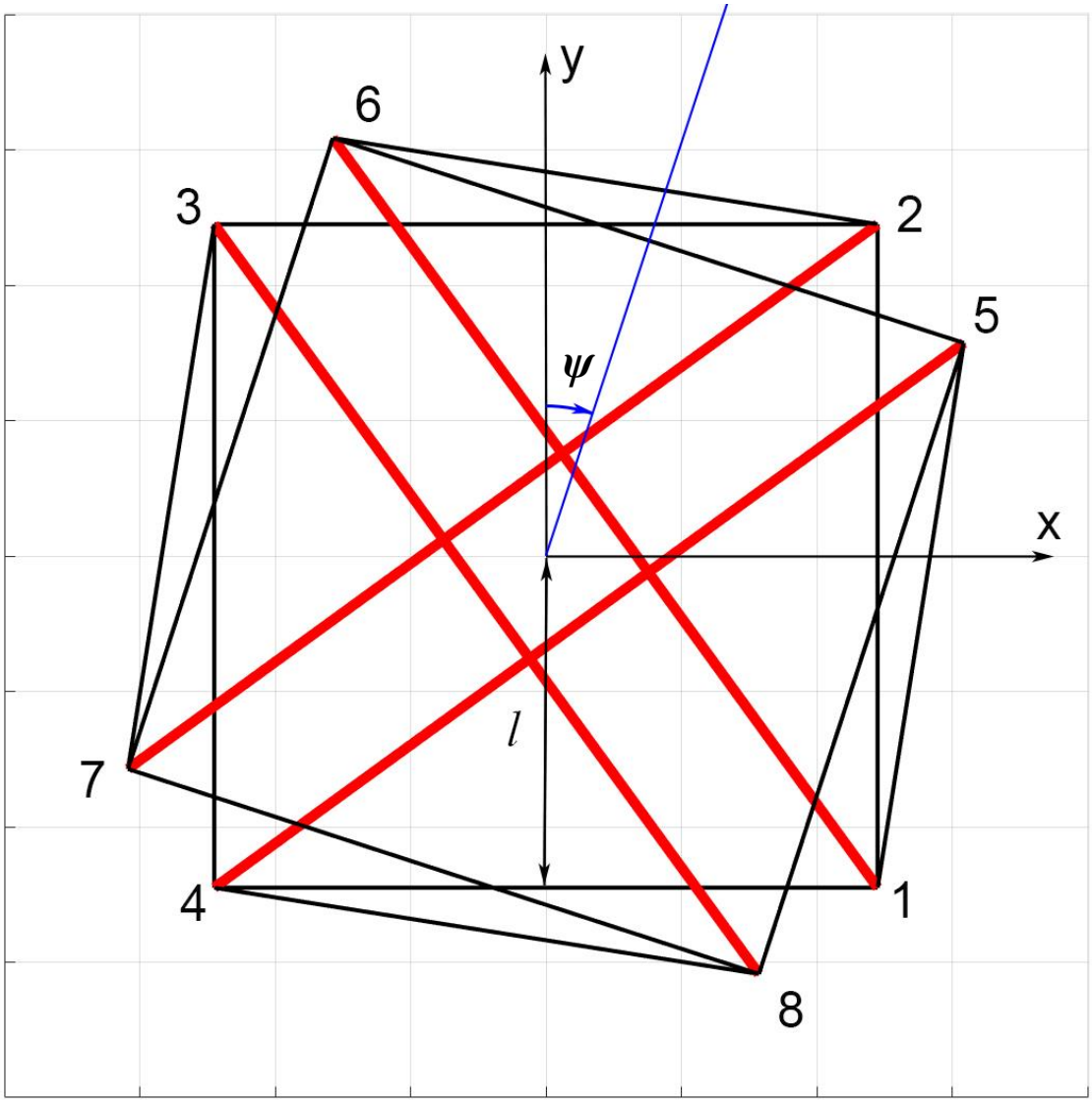

Figure 10. Top view. (PAIVA, KURKA and IZUKA, 2018)

$$N = \begin{bmatrix} l & l & -l & -l & l(c-s) & l(c+s) & l(s-c) & l(-c-s) \\ -l & l & l & -l & l(-c-s) & l(c-s) & l(c+s) & l(s-c) \\ 0 & 0 & 0 & 0 & h & h & h & h \end{bmatrix} \quad (1)$$

The length of a strut *b* is the distance between nodes 1 and 6, 2 and 7, 3 and 8 or 4 and 6, from this information the height *h* can be defined in function of the twist angle ψ (equation (2)). Similarly, the distance between nodes 1 and 5, 2 and 6, 3 and 7 or 4 and 8 is the length *v* of the inclined cables (equation (3)), finally defined in function of *ta* and *h* (which has just been defined in function of ψ).

$$h^2 = b^2 - l^2[(1-s+c)^2 + (1+s+c)^2] \quad (2)$$

$$v^2 = h^2 + l^2[(1-c+s)^2 + (c+s-1)^2] \quad (3)$$

3.3 Kinematics

The length of the inclined cable *v* and the height *h* were given in function of the twist angle *ta*. However, the only truly controllable variable is *v*, and the main objective in seeing how the height *h* changes with *v*, so this solution is not so useful yet, the idea for this section is calculating *v* and *h* for $0 < ta < \pi/4$ *rad*, then *h* vs. *v* can be plotted (Figure 11). Also, given a velocity for *v* of *-0.01m/s*, time *t* can be calculated, showing how the twist angle and the height change over time (Figure 12).

Finally, as *h* and *ta* are defined over time, the nodes positions *N* can be obtained (equation (1)) for all instants of time. With red lines representing the struts and black lines standing for the cables, an animation can be produced (Figure 13). There is a small displacement in the lower base between the struts and the wires, but that was inserted on purpose to reproduce the prototype (Figure 4). These results were obtained using *b=0.35m* and *l=0.1237m*.

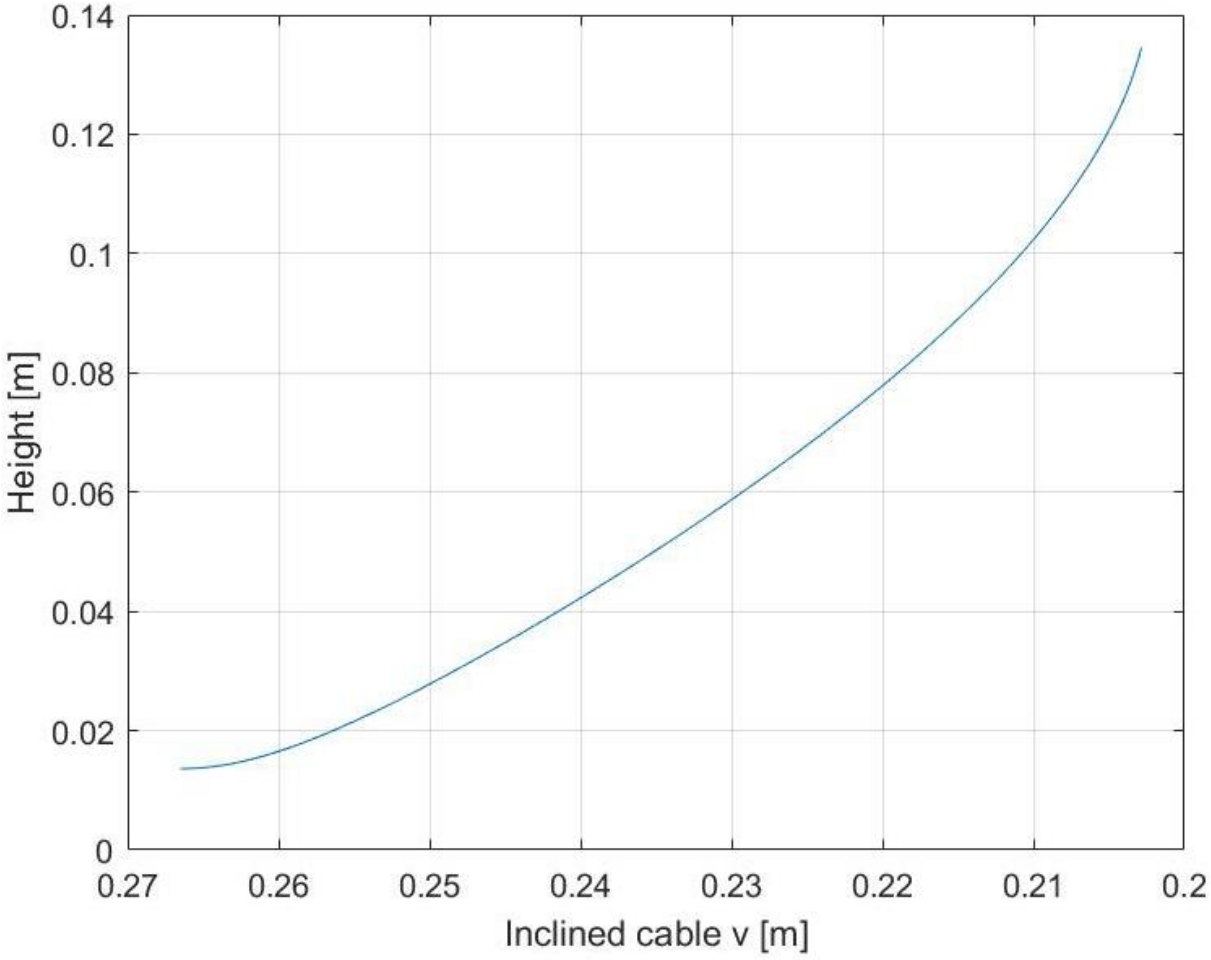

Figure 11. *h* vs. *v*. (PAIVA, KURKA and IZUKA, 2018)

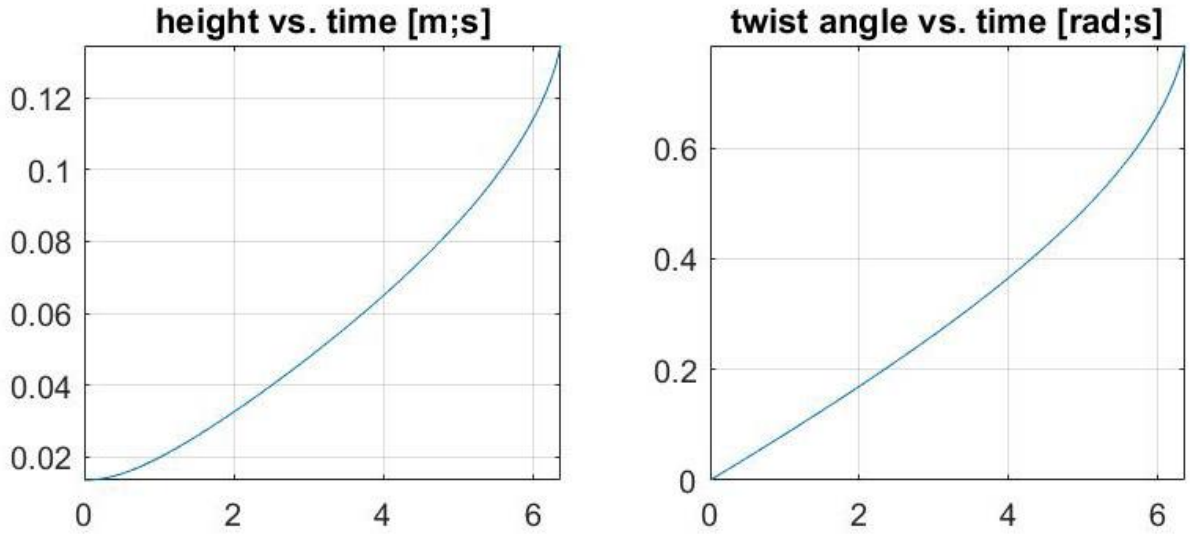

Figure 12. *ta* and *h* vs. *t*. (PAIVA, KURKA and IZUKA, 2018)

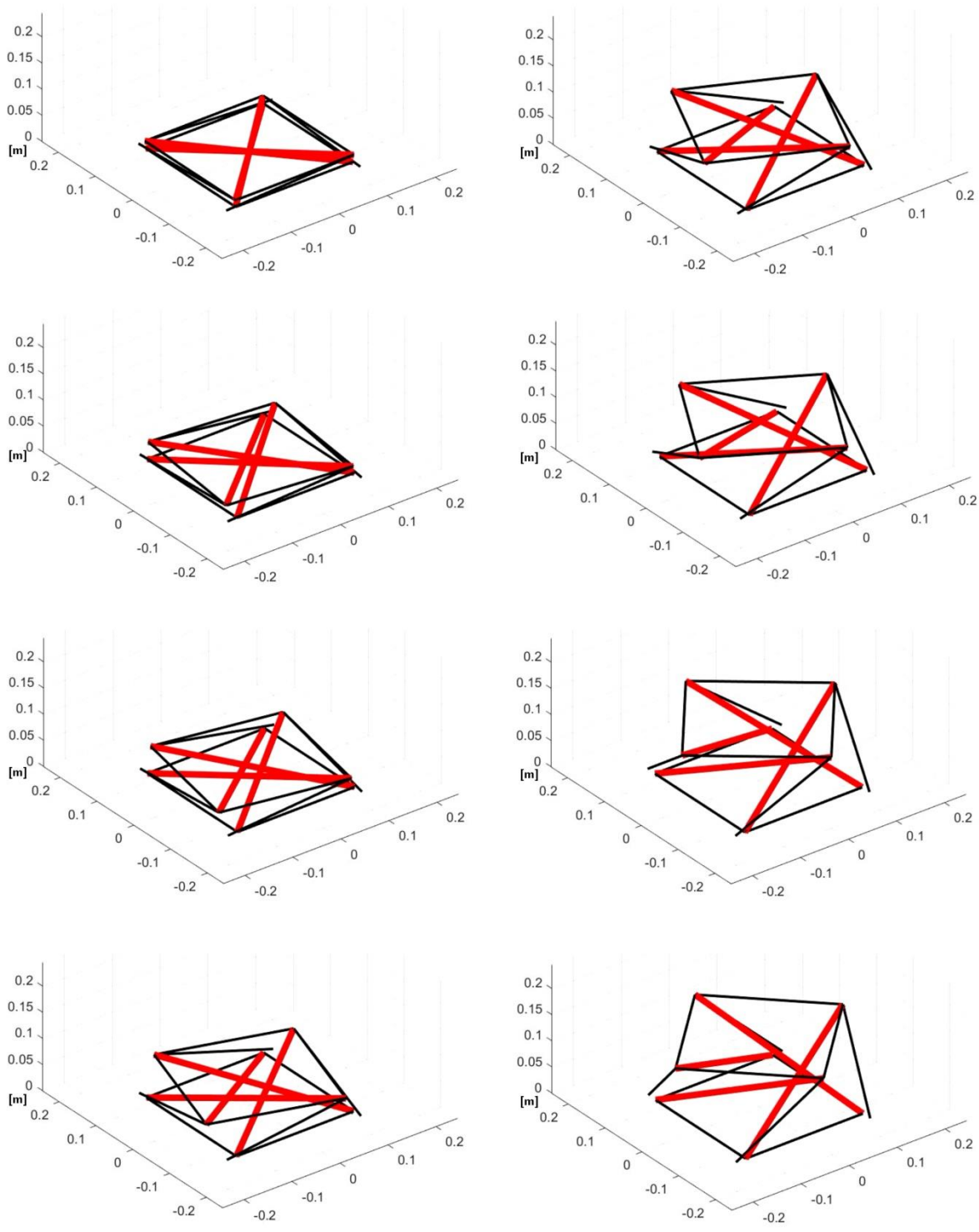

Figure 13. Expansion.

3.4 Discussion

A small pull in *v*, from *0.26m* to *0.2m*, causes a significant growth in *h*, from *0.02m* to 0.*14m* (Figure 11), so the first relevant characteristic of this mechanism is the high sensitivity of *h* to *v*. Another interesting feature is seeing the structure grow higher as the cables are pulled downwards, this can be considered counterintuitive, as people usually expect to see things become smaller after pulling it down.

The inclined cable was set to decrease linearly (*-0.01m/s*) over time, as *v* reduced approximately *0.06m*, the elapsed time should be around *6s*, which has been verified (Figure 12). Height increases with this reduction in *v*, the behaviour of *h* over time is just expected to be similar to *v*'s, but increasing instead, as confirmed in Figure 12. The same thought is valid to the twist angle, its variation from *0* to $\pi/4$ *rad* obeys equation (23) and follows a similar path over time comparing to *h*.

These characteristics match the expansion process detailed in Figure 13. By comparing the first and the last frame, the increase in height and twist angle and the decrease in the inclined cable are clear.

3.5 Validation

The movement of the structure was recorded by a *30fps* camera and analysed through the image processing software *Kinovea* (Figure 14). From a side view, the height and the pulling cable were tracked, and from the top view, the twist angle and the pulling cable were acquired. The positions acquired in pixels were converted to meters to plot the height (Figure 15), but since the twist angle ψ is dimensionless, this calibration was not necessary to calculate ψ from the top view and plot it versus *v* (Figure 16).

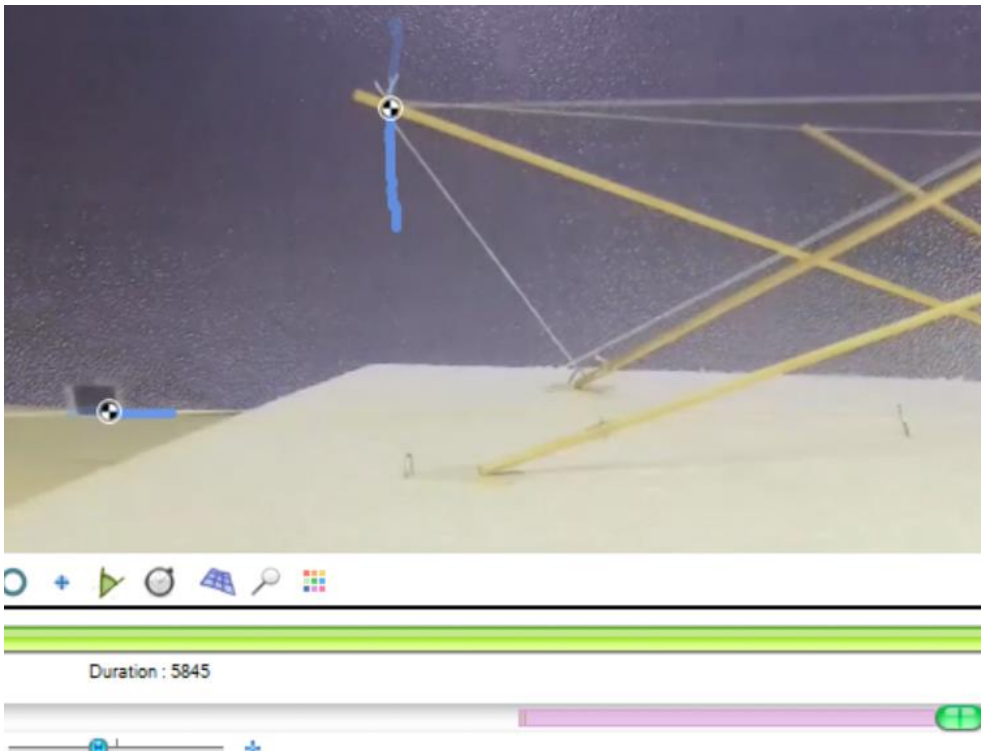

Figure 14. *Kinovea*. (PAIVA, KURKA and IZUKA, 2018)

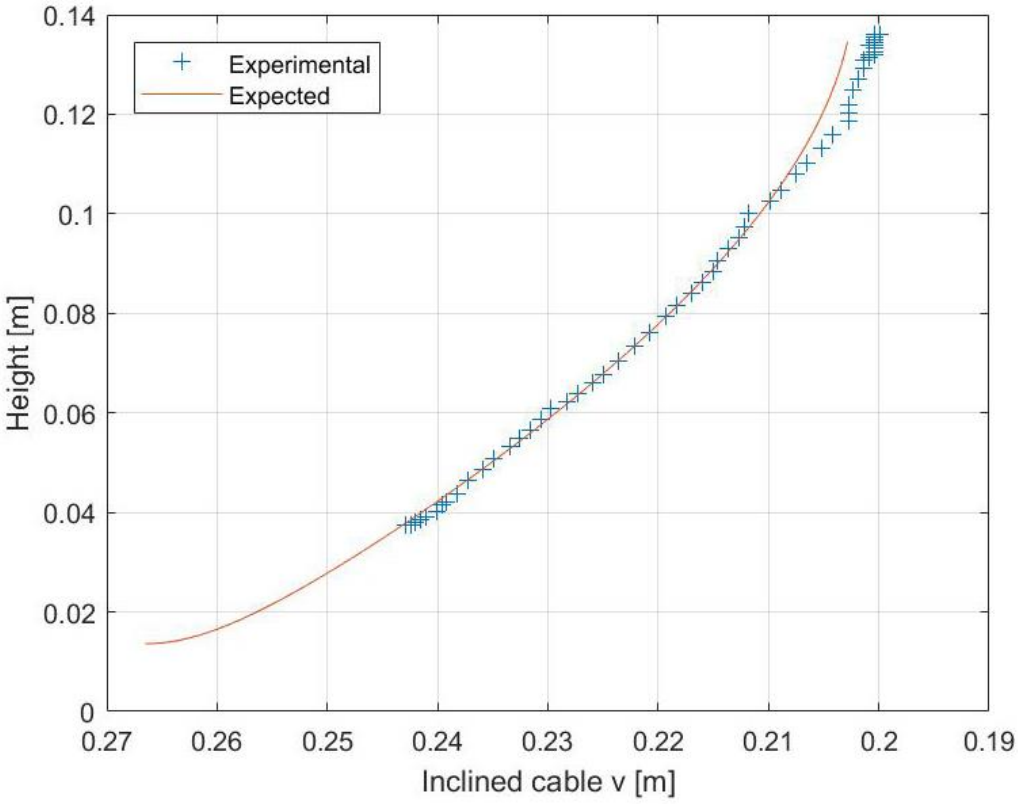

Figure 15. Height validation. (PAIVA, KURKA and IZUKA, 2018)

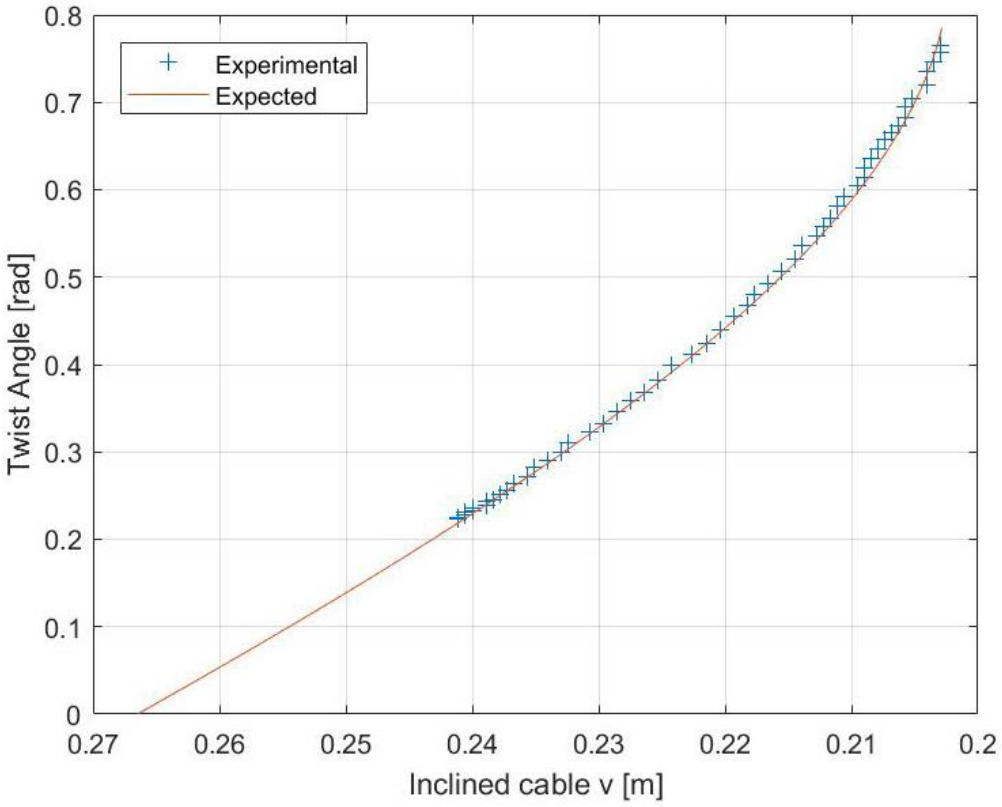

Figure 16. Twist angle validation. (PAIVA, KURKA and IZUKA, 2018)

The experimental points do not appear on the left hand side of the charts, this happens because the minimum height (and therefore the twist angle) of the prototype is never zero since the struts hit each other before hitting the ground, but in the simulation the bars trespass, enabling $h=0$. However, after reaching this minimum feasible height and twist angle, the simulations can be considered validated as more than *80%* of the experimental points matched precisely with the curve.

There is a noticeable difference between experimental points and simulation curve in the right hand side of the height chart. That deviation appeared because a small buckling of the bars happened in the end of the experiment due to the force required to lift the tensegrity, while in the simulations the struts were assumed to be *100%* rigid. These deformations lead to a greater displacement of the marker on the pulling cable, which is accidentally read as a reduction of v by the methodology, shifting the experimental points to the right. Furthermore, depth is not considered in the images analysis, as the twist angle grows a bit more sharply in the end, this approximation of a 3D structure in a 2D environment becomes less accurate from the side view, as objects look bigger when closer to the camera.

On the other hand, the effect of depth is less relevant when looking from the top view because all four tips of the struts are lifted at the same rate and the angle between them is not affected if all bars look bigger. So the twist angle data could be acquired more accurately, leading to an almost perfect match between the experiment and the expected results.

3.6 Energy Analysis

As there is no weight in space, the force required to lift the tensegrity is not so relevant, but the power of the engine may be important for other applications of this system. Given its symmetry, the traction necessary to lift the whole system is four times the force needed to lift one strut only. Neglecting the mass of the wires, the potential energy gained by the bar E_P (plus losses by friction E_F) equals the energy provided by the engine E_E (equation (4)), where m is the mass of a bar, F is the required force to lift the tensegrity (equation (5)) and F_F is the friction force. Finally, for a total time t and assuming the force is constant during the expansion process, the power $\dot{W}$ of the engine can be defined (equation (6)).

$$E_P + E_F = E_E \rightarrow 4mg\frac{h}{2} = (F_E - F_F)\Delta v \tag{4}$$

$$F_E = \frac{2mgh}{\Delta v} + F_F \tag{5}$$

$$\dot{W} = \frac{2mgh + F_F \cdot \Delta v}{t} \tag{6}$$

Some conclusions can be reached just from the equations, for example, tensegrities with more struts will have greater mass and height and lower Δv, leading to a higher engine power. To validate these definitions of engine force and power, known masses ($15g$ each) were attached to the struts and a scale was attached to the pulling cable, so the required force to hold the tensegrity up could be acquired (Figure 17). However, friction is helping the tensegrity to stand up in this case, so the sign of F_F in equation (5) must be inverted.

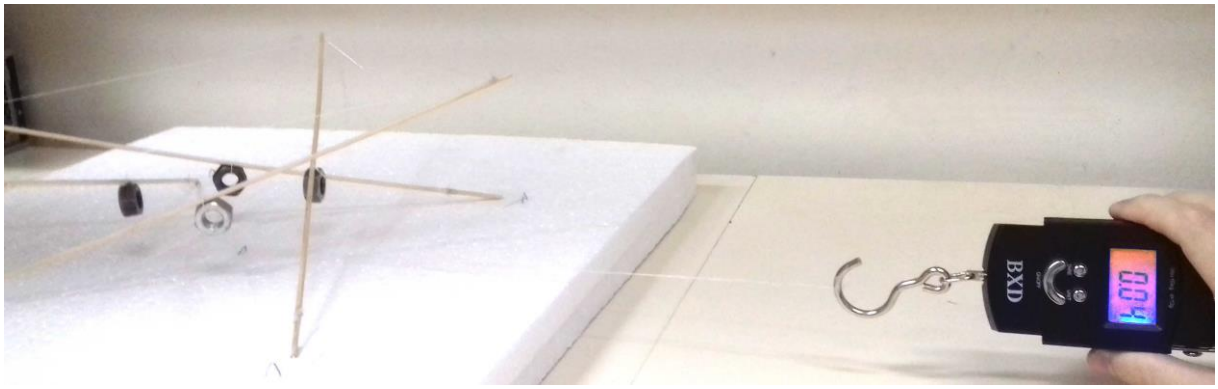

Figure 17. Force experiment. (PAIVA, KURKA and IZUKA, 2018)

One of the main challenges in this subsection is estimating the friction of the contact between clip and wire. Known masses were hanged by the wire through a clip, forming an acute angle, and the required force (W - F_F) to equilibrate the system was acquired by the scale (Table 1). When the angle formed by the wire around the clip is not acute, the friction forces can be neglected.

Table 1. Friction.

W [kgf]	W - F_F [kgf]	F_F/W
0.09	0.06	0.33
0.17	0.13	0.24
0.20	0.13	0.35
0.31	0.21	0.32
0.36	0.25	0.31
0.40	0.27	0.33
0.47	0.34	0.28
0.51	0.37	0.27
0.57	0.42	0.26

The friction forces bear an average of *29.8%* of the weight. In the prototype, 2 cables form only one contact clip wire that form an acute angle, so the force transmitted to the scale is *70.2%* of the traction before the clip. The other two cables are deformed by an acute angle twice, so the force transmitted to the scale is $(70.2\%)^2$ of the force before the first clip. The total force acquired by the scale (*0.04 kgf*) is the sum of all 4 cables after passing through the last clip (equation (7)).

$$F_E = \frac{mg}{\Delta v}\frac{h}{2}[2 \cdot 70.2\% + 2(70.2\%)^2] \rightarrow$$
$$\rightarrow F_E = \frac{0.015 \cdot 9.81}{0.06} \cdot \frac{0.137}{2} \cdot 2.4 = 0.42N = 0.042kgf \quad (7)$$

3.7 Conclusions

A 4 struts class 1 tensegrity had its expansion process simulated, verified and studied. The experimental data was acquired by a 2D image processing software, but the experiment is 3D with clearly large displacements, so a small portion of the experimental results was compromised because objects closer to the camera look bigger. Still, more than *80%* of the experimental points matched perfectly with the numerical results. The analysis lead to a better understanding of the experimental process and highlighted certain characteristics, such as the high sensitivity of the height to the pull of the inclined cable, or how the twist angle changes as the structure grows taller.

The engine force and power were defined by an energy analysis, which was also validated through an experiment. Known masses were attached to the bars so they had relevant inertias and the force to keep the structure up was acquired by a scale. Some assumptions and approximations regarding the friction forces were necessary, but the results matched in the end, endorsing the assumptions and the energy analysis overall.

The reflector surface could also be replaced by a membrane made of a reflective material, this would reduce the mass of the system. Future steps for this study include the definition of a tensegrity-membrane model and the characterization of the behaviour of the

membrane itself. Another possible extension of this work could be a class 2 tensegrity tower made of several modules of the mechanism shown in this chapter on top of each other, to be used as a manipulator arm.

Finally, the system studied in this chapter can be sent to space in a compact configuration, easily sustaining the loads of the launch and saving volume in the rocket. Then the tensegrity is expanded on orbit, reaching its maximum height after a small pull of the inclined cables, putting the reflector surface as far as it needs to be from the satellite's wall to avoid the generation of noise. When comparing to the traditional solid cone that supports the antennas nowadays, the mass of this system is lower and, after completely expanded, its stiffness can be controlled as studied in chapter 3, adding one more useful feature to this potential stand of a satellite antenna.

4 PRE-STRESS AND STIFFNESS

The stiffness of a tensegrity structure can be controlled without altering the shape if the pre-stresses of all cables are proportionally changed. This property was analysed on a 3 bars and 9 cables tensegrity prism. Firstly the stiffness of a member was found given its pre-stress and then the global stiffness of the structure is calculated using the methodology based on Skelton's (2009) work. Then, a modal analysis was performed on the structure and finally the sensitivity of the natural frequencies to the pre-stress was checked. A prototype (Figure 5) was built to validate the methodology.

Despite not having an immediate application, the design suggested in this chapter is valuable as a first step into calculating the stiffness of a tensegrity. This initial stage is recommended to better understand the methodology (which will be used again in chapter 5) with a simple and easy to visualize model.

4.1 Finding the pre-stresses

Assuming the pre-stress does not deform the members and the structure is static, the pre-stresses of the members can be found through nodes method (HIBBELER, 2004). As if the tensegrity were a truss: the sum of forces in each node is equal to zero (equation (8)).

$$\begin{aligned} \sum F_x &= 0 \\ \sum F_y &= 0 \\ \sum F_z &= 0 \end{aligned} \tag{8}$$

This method is convenient for this study because the structure is symmetric, so one single node is enough to find the forces. The pre-stress σ_k and the force density s_k of the members are defined in equations (9) and (10), where F_k is the axial force, A_k is the cross-section area and L_k is the length of the element k.

$$\sigma_k = \frac{F_k}{A_k} \tag{9}$$

$$s_k = \frac{F_k}{L_k} \tag{10}$$

4.2 Stiffness of a member

Based on the model suggested by Skelton (2009), the position n_i of the i^{th} node of the structure is defined in equation (11) and the nodes matrix N in equation (12), where n is the number of nodes of the structure:

$$n_i = \begin{Bmatrix} x_i \\ y_i \\ z_i \end{Bmatrix} \tag{11}$$

$$N = [n_1 \quad n_2 \quad \dots n_n] \tag{12}$$

The connectivity c_k of a member k that connects nodes i and j is given by equation (13), where e_i is a vertical vector filled with zeros except in the i^{th} position, whose value is *1*. The connectivity matrix C is formed by the connectivity vectors of all members (equation (14), where m is the number of members) and the members matrix is shown in equation (15).

$$c_k = e_i - e_j \tag{13}$$

$$C^T = [c_1 \quad c_2 \quad \dots \quad c_m] \tag{14}$$

$$M = NC^T = [m_1 \quad m_2 \quad \dots \quad m_m] \tag{15}$$

The stiffness K_k (equation (16)) of a member k can be obtained from the connectivity vectors c_k and the matrix S_k (equation (17)) through a Kronecker product (Appendix B). S_k is

calculated from the column m_k of the members matrix M and from the force density s_k of the respective member. The first term is the contribution of the pre-stress and the second is related to the material. Because the forces come from linear elastic elements in this work, K_B is the stiffness of the material, defined in equation (18) for bars.

$$K_k = c_k c_k^T \otimes S_k \tag{16}$$

$$S_k = s_k \left(I_3 - \frac{m_k m_k^T}{\|m_k\|^2} \right) + K_B \cdot \frac{m_k m_k^T}{\|m_k\|^2} \tag{17}$$

$$K_B = \frac{EA}{L} \tag{18}$$

4.3 Modal analysis

The mass matrix of a bar element (Figure 18) is given by equation (19) where *le* is the length of the element and *φ(x)* (equation (20)) is a shape function (COOK, 1995) of first order.

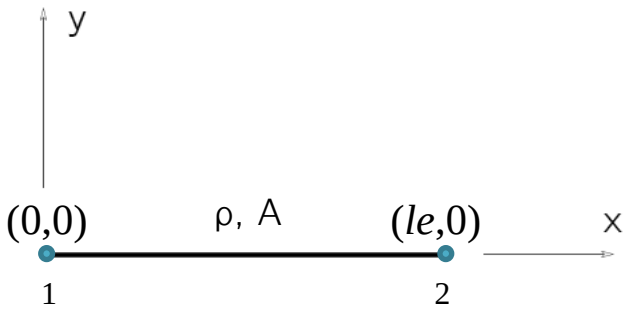

Figure 18. Bar element for mass matrix.

$$M_e = \int_0^{le} \rho[\varphi(x)^T \varphi(x)]\, dV \tag{19}$$

$$\varphi(x) = \begin{bmatrix} 1 - \frac{x}{le} & 0 & \frac{x}{le} & 0 \\ 0 & 1 - \frac{x}{le} & 0 & \frac{x}{le} \end{bmatrix} \tag{20}$$

Solving equation (19), the mass matrix of an element (equation (21)) is obtained:

$$H_k = \frac{\rho \cdot A \cdot le}{6} \begin{bmatrix} 2 & 0 & 1 & 0 \\ 0 & 2 & 0 & 1 \\ 1 & 0 & 2 & 0 \\ 0 & 1 & 0 & 2 \end{bmatrix} \tag{21}$$

The global mass matrix H_G is obtained through superposition of the elements' mass matrices H_k. Then, the natural frequencies ω and their respective modes of vibration $\{d\}$ can be calculated (equation (22)) (BATHE, 1996).

$$([K_G] - \omega^2 \cdot [H_G]) \cdot \{d\} = 0 \tag{22}$$

4.4 Definition of the model

A tensegrity prism with 3 struts (thick lines) and 9 cables (thin lines) is analysed in this chapter (Figure 19). The lower base is formed by nodes 1, 2 and 3, while the upper base is formed by nodes 4, 5 and 6. The geometrical parameters of the model are *h=0.12m* of height and *l=0.12m* of base side. The cross section of the strut is square with *6mm* side and the cross section of the cable is round with *0.33mm* diameter. Density is *1200kg/m³* for both materials and Young modulus is *3GPa* for the bar and *2GPa* for the cable.

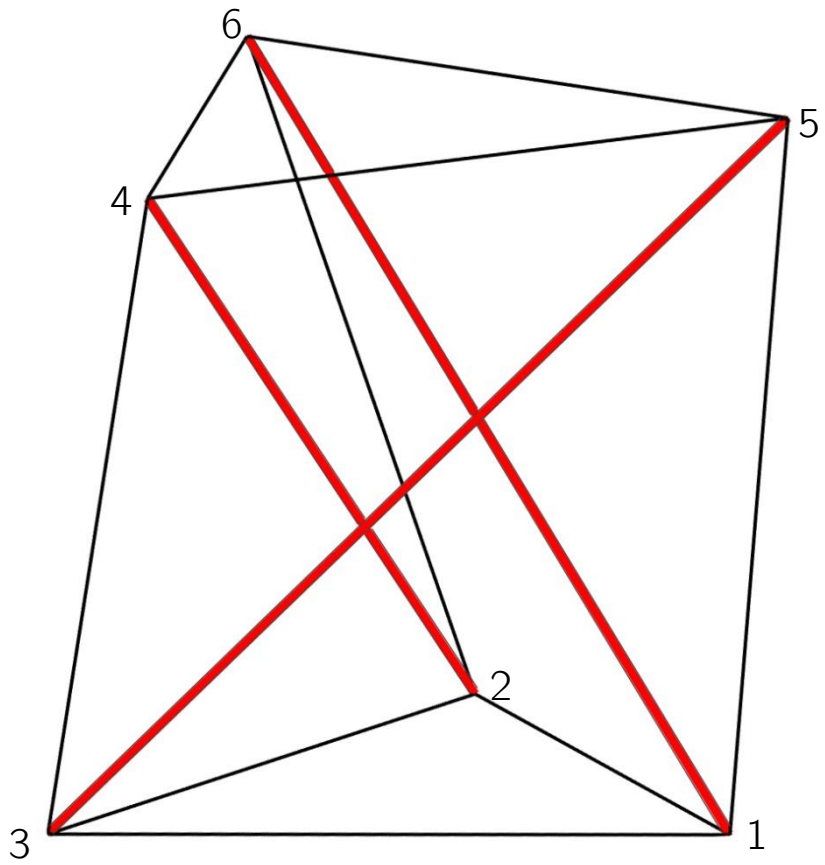

Figure 19. Tensegrity prism.

The angle ψ between the two bases seen from the top view (Figure 20) is called twist angle and may be variable in a mechanism (as in chapter 3). For a tensegrity prism, its maximum value ψ_s depends on the number of struts n_s (equation (23)) and the mechanism turns into a static structure once $\psi = \psi_s$. If an extra tension is applied, the shape will not change anymore but the stiffness will increase.

$$\psi_s = \frac{\pi}{2} - \frac{\pi}{n_s} \tag{23}$$

For example, a tensegrity prism with 6 struts becomes static when $\psi = 60°$ and a 4 struts prism stabilizes when $\psi = 45°$, which matches the last value ($\psi = 0.785\ rad = 45°$) of Figure 16.

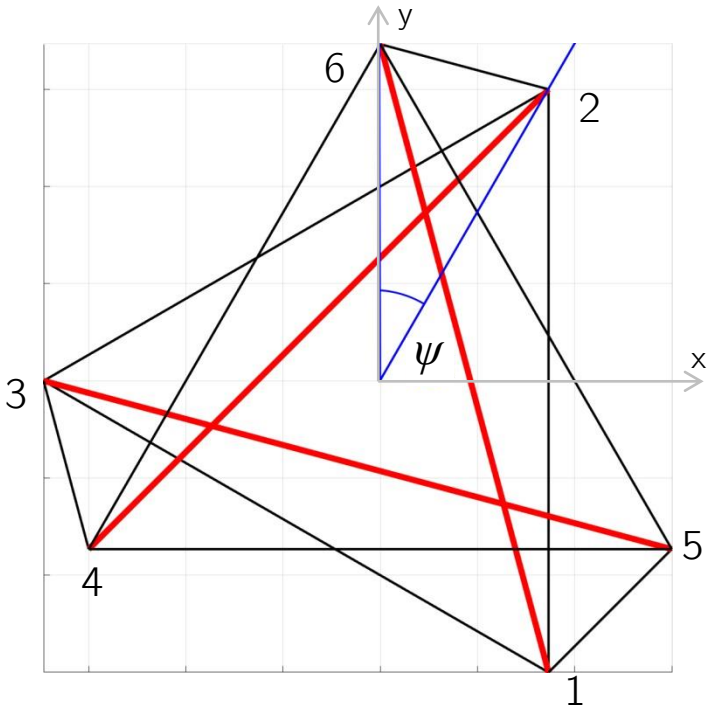

Figure 20. Top view.

In this tensegrity prism, the number of struts is n_s=*3*, which leads to a twist angle of *30°* and enables the calculation of the nodes positions and connectivity matrix (equations (24), (25) and (26)).

$$n_1 = \begin{bmatrix} \frac{l}{6}\sqrt{3} \\ -\frac{l}{2} \\ 0 \end{bmatrix} \quad n_2 = \begin{bmatrix} \frac{l}{6}\sqrt{3} \\ \frac{l}{2} \\ 0 \end{bmatrix} \quad n_3 = \begin{bmatrix} -\frac{l}{3}\sqrt{3} \\ 0 \\ 0 \end{bmatrix}$$

$$n_4 = \begin{bmatrix} \frac{l}{2} \\ -\frac{l}{6}\sqrt{3} \\ h \end{bmatrix} \quad n_5 = \begin{bmatrix} -\frac{l}{2} \\ -\frac{l}{6}\sqrt{3} \\ h \end{bmatrix} \quad n_6 = \begin{bmatrix} 0 \\ \frac{l}{3}\sqrt{3} \\ h \end{bmatrix} \tag{24}$$

$$N = [n_1 \quad n_2 \quad n_3 \quad n_4 \quad n_5 \quad n_6] \tag{25}$$

$$C = \begin{bmatrix} -1 & 0 & 0 & 0 & 0 & 1 \\ 0 & -1 & 0 & 0 & 1 & 0 \\ 0 & 0 & -1 & 1 & 0 & 0 \\ -1 & 1 & 0 & 0 & 0 & 0 \\ 0 & -1 & 1 & 0 & 0 & 0 \\ 1 & 0 & -1 & 0 & 0 & 0 \\ 0 & 0 & 0 & -1 & 1 & 0 \\ 0 & 0 & 0 & 0 & -1 & 1 \\ 0 & 0 & 0 & 1 & 0 & -1 \\ -1 & 0 & 0 & 1 & 0 & 0 \\ 0 & -1 & 0 & 0 & 0 & 1 \\ 0 & 0 & -1 & 0 & 1 & 0 \end{bmatrix} \begin{matrix} n_1 \to n_6 \\ n_2 \to n_5 \\ n_3 \to n_4 \\ n_1 \to n_2 \\ n_2 \to n_3 \\ n_3 \to n_1 \\ n_4 \to n_5 \\ n_5 \to n_6 \\ n_6 \to n_4 \\ n_1 \to n_4 \\ n_2 \to n_6 \\ n_3 \to n_5 \end{matrix} \quad (26)$$

By symmetry, all the 6 horizontal cables are under the same pre-tension τ_H, the 3 cables connecting both bases are under τ_V and the bars under τ_B. From equation (8), by assuming one of those three pre-tensions (τ_H, τ_B or τ_V), the other two can be found. Then the stiffness can be calculated from equation (17) for each combination of tensions and, finally, the natural frequencies and modes of vibration (Figure 35, Figure 36 and Figure 37 in Appendix (A) can be found from equation (22). The mass matrix does not change with the pre-stresses.

4.5 Validating the model with a FEA software

Using the *inistate* command for the pre-stresses and the *link180* element on Ansys APDL, the same model was analysed (Figure 21) and the results were compared to those obtained from the methodology described in this chapter (Table 2). The rigid body modes are not available in the table or in Figure 35, Figure 36 and Figure 37.

The stiffness increases with the pre-stresses. As the natural frequencies are positively related to the stiffness, it is just expected that the natural frequencies should increase with the pre-stresses too, this behaviour was confirmed with the simulations. Additionally, the values matched with the commercial software, enhancing the reliability of the methodology described in this chapter and qualifying the study to advance to the experimental procedures.

Table 2. Natural frequencies [Hz].

	τ_H = 0 [N]		τ_H = 10 [N]		τ_H = 20 [N]	
Mode	Ansys	Model	Ansys	Model	Ansys	Model
1	1.96E-05	1.88E-05	57.5	57.5	81.3	81.3
2	117.8	117.8	126.5	126.5	134.3	134.3
3	117.8	117.8	126.5	126.5	134.3	134.3
4	149.6	149.6	154.3	154.3	158.8	158.8
5	149.6	149.6	154.3	154.3	158.8	158.8
6	217.5	217.5	221.7	221.7	225.8	225.8
7	245.0	245.0	242.1	242.1	239.5	239.5
8	245.0	245.0	242.1	242.1	239.5	239.5
9	293.9	293.9	286.4	286.4	278.7	278.7
10	3944.4	3944.4	3945.0	3945.0	3945.5	3945.5
11	3944.4	3944.4	3945.0	3945.0	3945.5	3945.5
12	3953.8	3953.8	3953.8	3953.8	3953.9	3953.9

The normal force of the other cables τ_V and bars τ_B were found through equilibrium of forces as shown in equation (8) and the pre-stresses of the cables and bars were calculated given the cross-section areas of the elements.

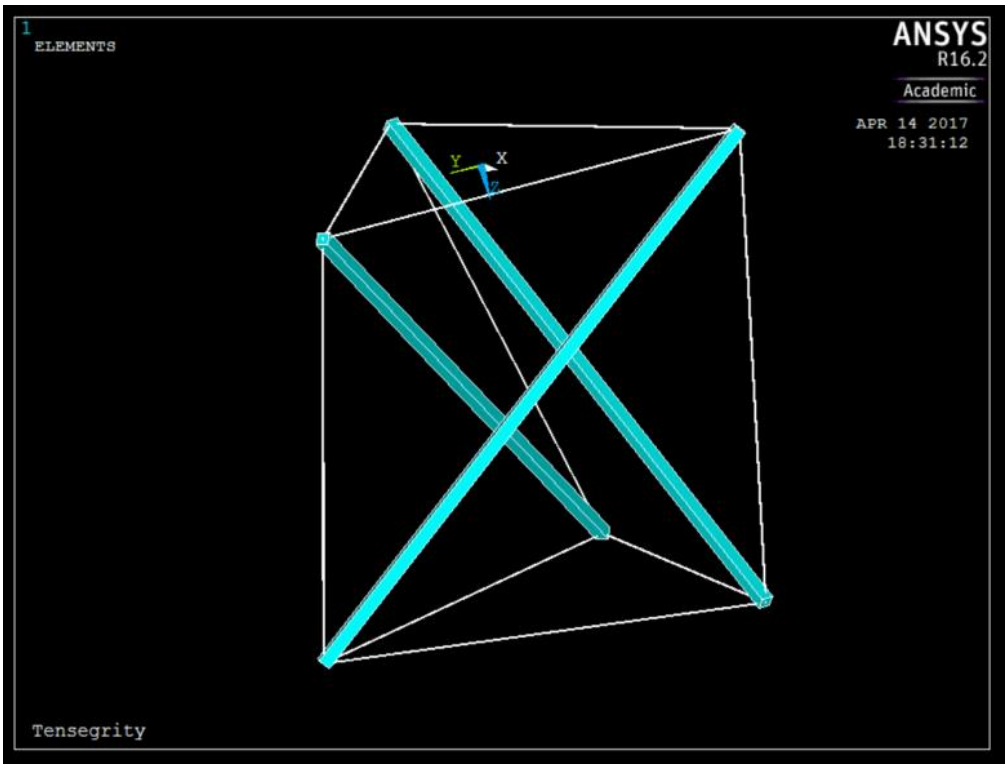

Figure 21. Ansys model.

4.6 Prototype and tensiometer

With $h=0.13m$ and $l=0.12m$, the prototype (Figure 5) was built with steel struts (approximately $200GPa$ of Young modulus, $8400kg/m^3$ of density and square cross section of $6.3mm$ side) and nylon cables (approximately $3GPa$ of Young modulus, $1200kg/m^3$ of density and round cross section of $0.4mm$ diameter). The magnified detail (Figure 22) shows how the pre-stresses can be manipulated by the torque applied on the screws.

A relevant complication with this experiment was measuring the tension to which the cables were subjected, to solve this issue a wire tensiometer was built (Figure 23). The force P required to transform the cable into the shape of the instrument is acquired by the scale, as that geometry is known, the traction of the cable can be calculated. Using the symbols shown in the scheme (Figure 24), the angle Θ is given in function of a and b in equation (27) and the traction T is found in terms of force P in equation (28).

$$tg(\theta) = \frac{a}{2b} \rightarrow \theta = arctg\left(\frac{a}{2}b\right) \tag{27}$$

$$2T \cdot cos(\theta) = Pg \rightarrow T = \frac{Pg}{2 \cdot cos\left(arctg\left(\frac{a}{2}b\right)\right)} \tag{28}$$

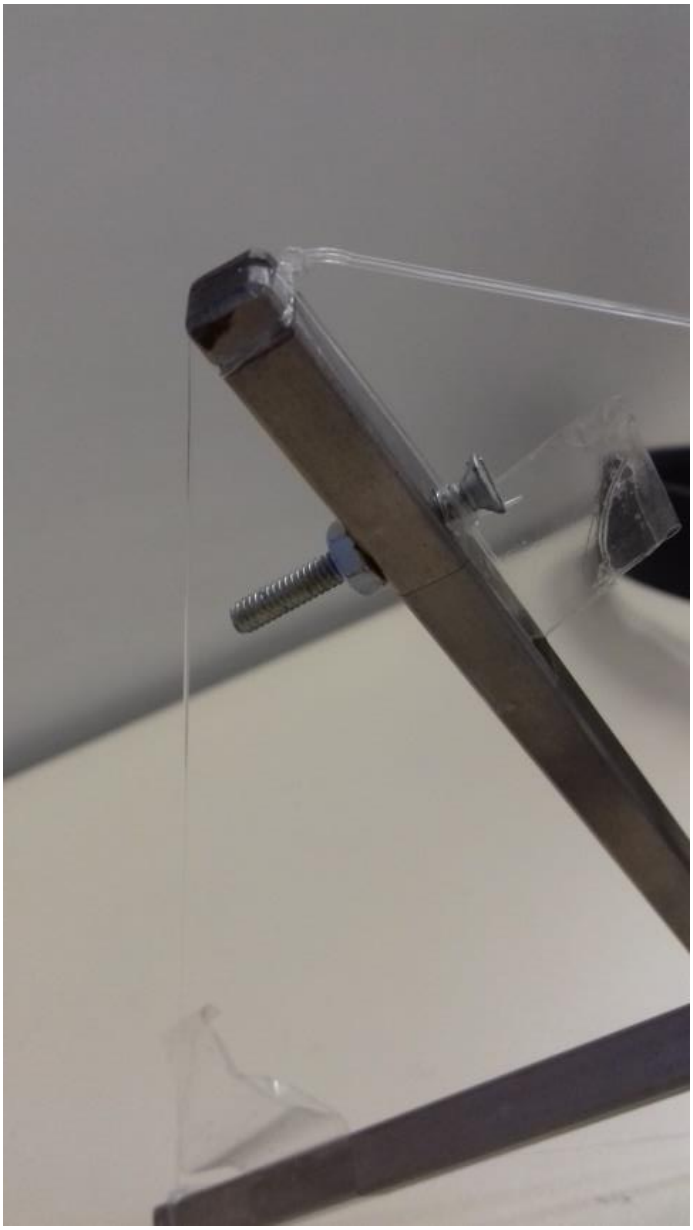

Figure 22. Detail of the prototype 1.

Figure 23. Wire tensiometer.

However, the cable had to be deformed to shape that triangle in Figure 24, generating some extra traction due to the elongation of the cable. Given the area *A* of the cross section, the total length L_T and the Young modulus *E*, the extra traction τ_E is defined in equation (29), and the correction is applied in equation (30).

$$\Delta L = \sqrt{\frac{1}{4}b^2 + a^2} - b$$
$$\tau_E = \Delta L \cdot \frac{EA}{L_T} \rightarrow \tau_E = \left(\sqrt{\frac{1}{4}b^2 + a^2} - L\right) \cdot \frac{EA}{L_T} \quad (29)$$

$$T = \frac{Pg}{2 \cdot cos\left(arctg\left(\frac{a}{2}b\right)\right)} - \left(\sqrt{\frac{1}{4}b^2 + a^2} - b\right) \cdot \frac{EA}{L_T} \quad (30)$$

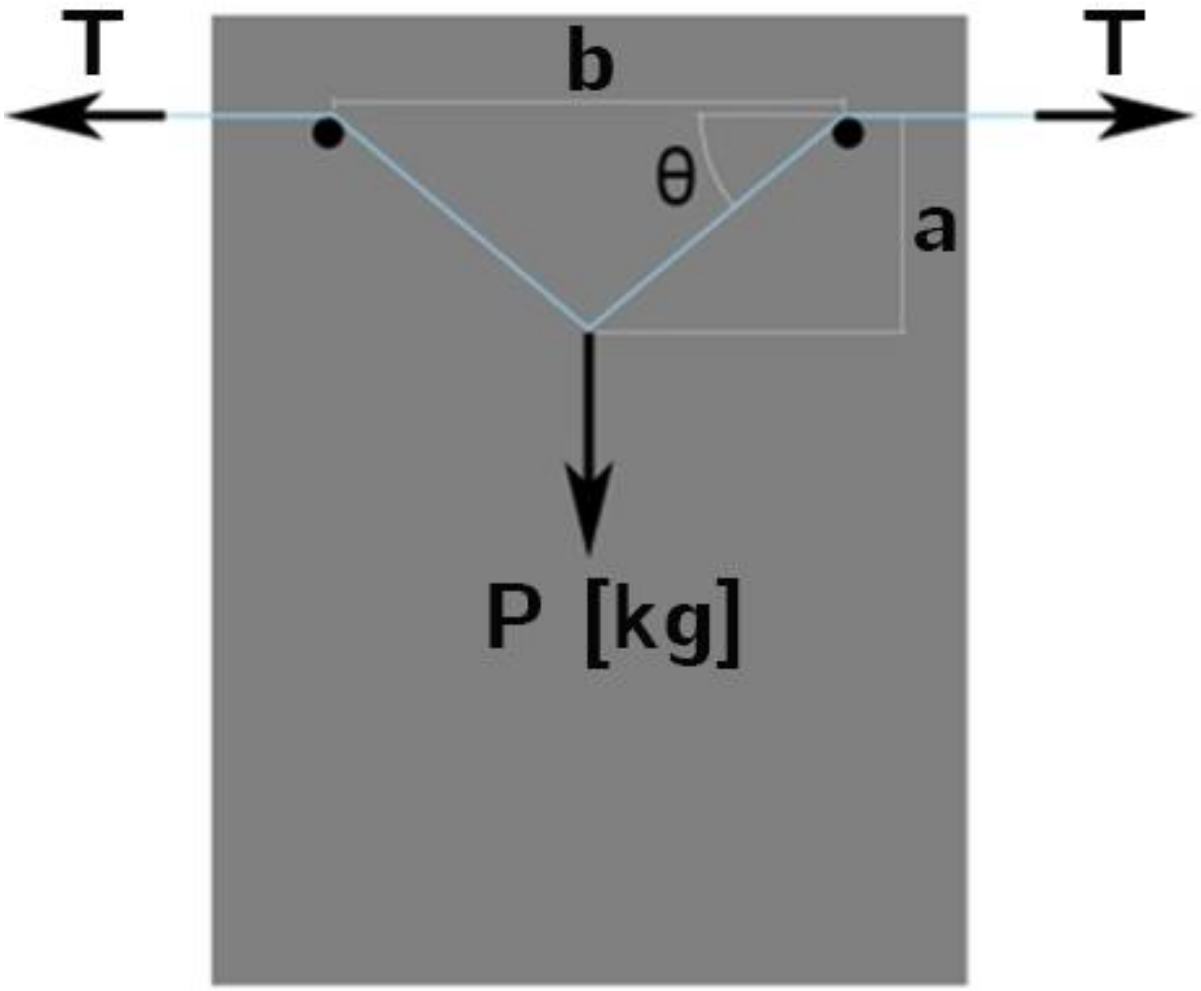

Figure 24. Tensiometer scheme.

This result is valid when both ends of the cable are fixed and the only way to form the triangle is by stretching the wire. However, in the prototype, the ends are not fixed, an effective approach to minimize this error is selecting values for *a* and *b* that make τ_E irrelevant. Using the estimated properties of our cable, *a=0.007m*, *b=0.09m* and L_T*=0.12m*, the influence of this additional traction is small enough (Figure 25) compared to the actual traction. The least count and maximum weight the scale can acquire are *10g* and *50kg* respectively.

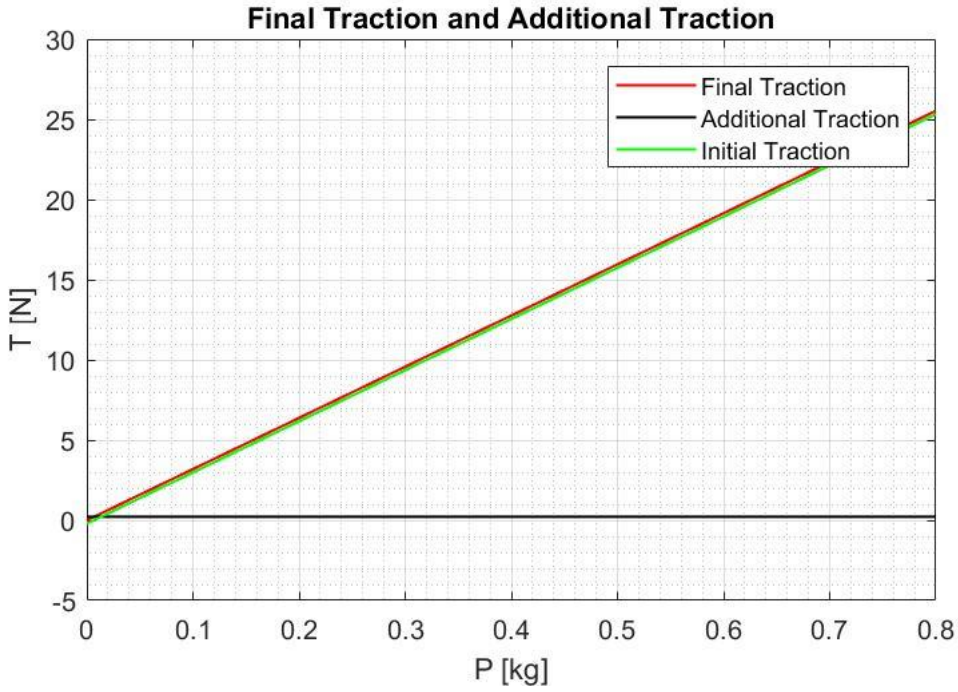

Figure 25. Tractions.

4.7 Experimental modal analysis

The inaccuracies related to the concentrated mass of the screws were minimized by positioning the prototype with the screws close to the ground. A *30fps* camera recorded the vibration of the structure after an external step input in one of the struts, the video was analysed in the image processing software *Kinovea* (Figure 26) to obtain the position of the tip of a bar every *33ms*. The frequency response was obtained through discrete Fourier transform using the *fft()* command in MATLAB.

The experiment was repeated for three different sets of pre-tension: $\tau_{H1}=1.8N$, $\tau_{H2}=3.3N$ and $\tau_{H3}=4.3N$ (Figure 27). The displacements were measured in pixels and were not converted to meters because the focus of this chapter is finding the natural frequencies, therefore calibration is not necessary in this section. The numerical model was adapted to reproduce the dimensions and restrictions of the prototype, the results are available in Table 3.

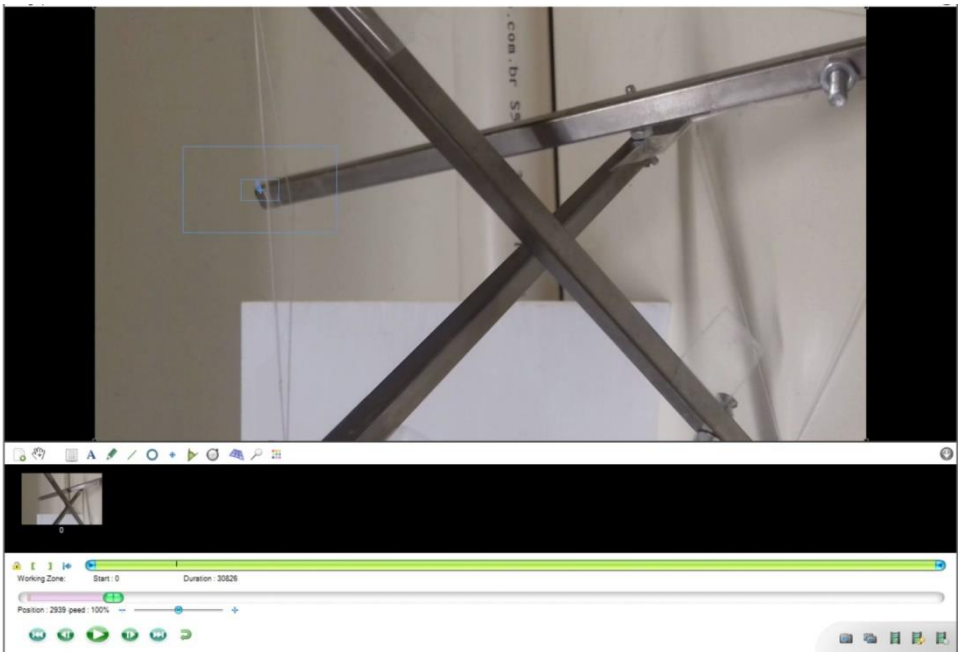

Figure 26. *Kinovea*.

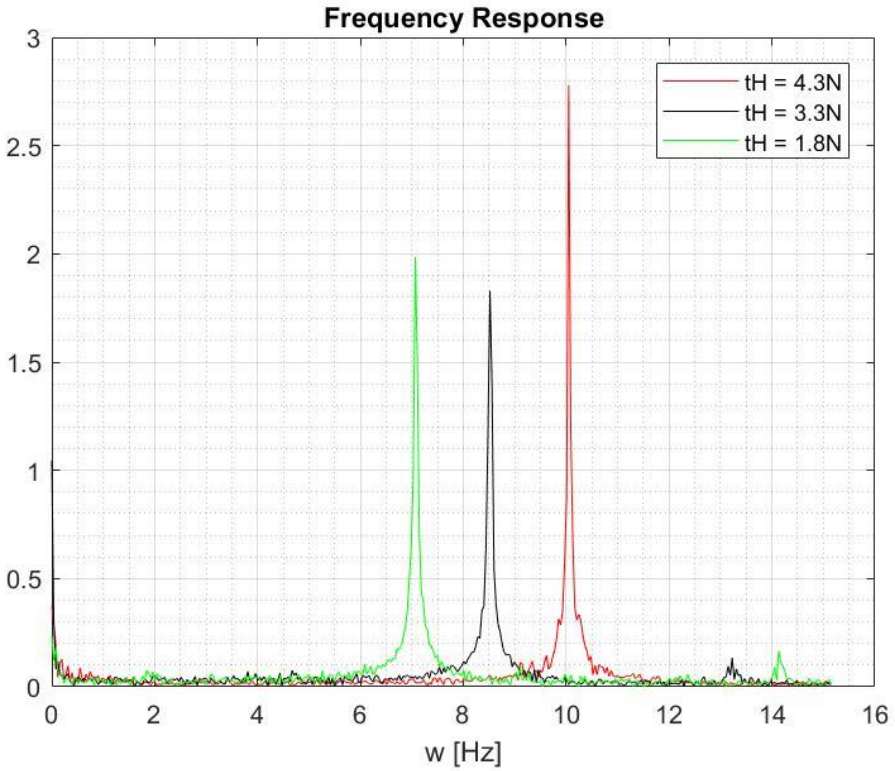

Figure 27. First natural frequencies.

Table 3. First natural frequencies comparison.

Traction τ_H [N]	1.8	3.3	4.3
Prototype [Hz]	7.07	8.52	10.1
Model [Hz]	7.16	9.69	11.07
Error	1.3%	12.1%	9.2%

4.8 Conclusions

Based on Skelton's (2009) results, a methodology was suggested to calculate the stiffness of a pre-tensioned tensegrity and determine its vibrational behaviour. A prototype was built with metallic struts and nylon cables and subjected to modal analyses under different pre-stresses to compare with the numerical results, which agreed overall.

Many challenges appeared regarding the construction, for example, screws had to be attached to the tips of the bars so the pre-stresses could be controlled and an instrument was built to measure the traction forces in the tendons.

The inaccuracy is more relevant with greater tensions (Table 3), that happens mainly because the prototype is not perfectly symmetric, and these asymmetries are enlarged with greater pre-tensions. However, the purpose of verifying that increased pre-stresses lead to a higher stiffness was achieved, as well as validating the methodology, so the main targets of this chapter were reached.

5 NONLINEAR STATIC DEFORMATION

The use of a long mast on top of a space exploration probe assists the acquisition of data from a higher spot (thus allowing the observation of a farther horizon), and a bendable structure enables the investigation of unreachable places such as holes. The design suggested in this chapter is an alternative to the long and flexible beam proposed by Kurka (2014), with adapted methodologies to perform similar static and modal analyses on tensegrities.

The stiffness matrix found by the methodology described in the previous chapter may be used to find the deformation *{x}* of the structure given a load vector *{F}* (equation (31)).

$$\{F\} = K_G\{x\} \rightarrow \{x\} = K_G^{-1}\{F\} \tag{31}$$

However, for large deformations, the nodes matrix *N* changes and so does the stiffness matrix K_G, therefore the problem becomes nonlinear. There are several ways for calculating large displacements, the incremental loads (or Euler's) method (CRISFIELD, 2000) is not the most efficient, but was chosen for being simple and suiting the requirements of this analysis. The objective of this chapter is to define a methodology for tensegrities under large deformations by combining Euler's method for large displacements with the methodology based on Skelton's (2009) work for linear tensegrities. Finally, a prototype (Figure 6) was built to validate the experiments and the natural frequencies of the deformed positions were calculated and analysed.

5.1 Incremental loads

For a given force *F* that causes large deformations on the structure, Euler's method consists in applying *p* small increments of *F/p* so the deformations are small enough to make the analysis linear. However, the stiffness has to be updated every step with the new positions of the nodes. In this work, the stiffness is updated considering not only the new nodes positions, but the new stresses of the members as well.

The cross section areas *A*, the incidence of the members and the materials properties *E* and ρ and are assumed to be always constant, represented by dotted lines in Figure 28. The incremental load stays in a dashed box because its module *F/p* is constant, but the direction may change, and the other parameters are squared by solid lines because they vary every step.

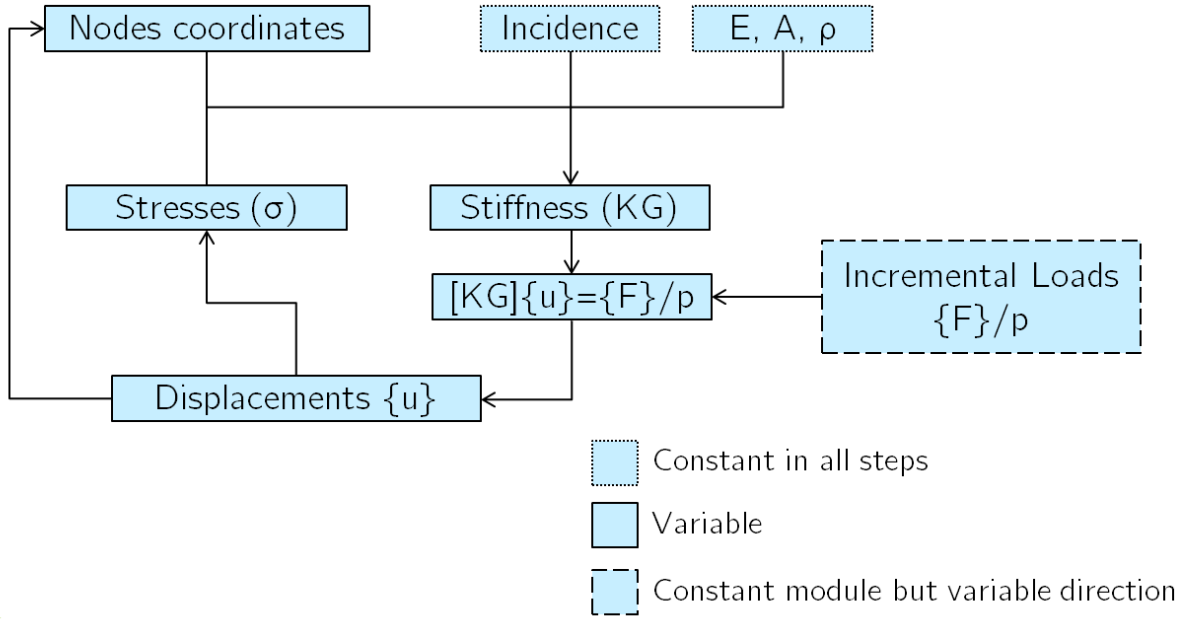

Figure 28. Incremental loads flow chart.

5.2 Description of the system

A bi-dimensional tensegrity tower (Figure 29) is the focus of this chapter. As the maximum number of rigid bodies in contact is 2, it is a class 2 tensegrity. The six levels structure has its base fixed and the top right tip attached to a point close to the base by a cable, which is pulled making the system bend likewise a fishing rod. The thick lines represent the bars and the thin lines represent the cables.

Subjected to different loads, a goal of this chapter is predicting the behaviour of the structure with the presented methodology and comparing with the results of the prototype. Gravity is considered but the prototype had to be hanged upside down to remain bi-dimensional, so the weight points upwards in Figure 29.

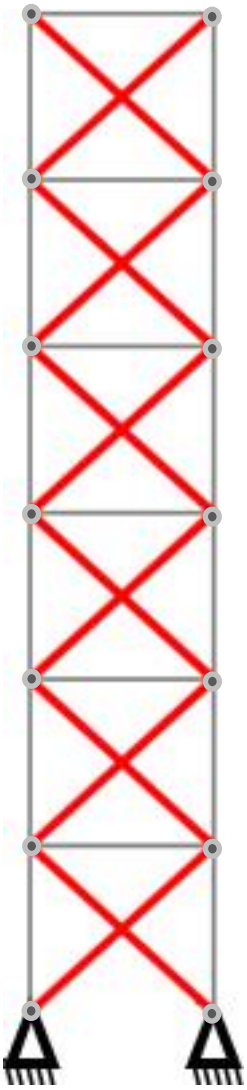

Figure 29. 2D tensegrity tower.

5.3 Materials properties

The struts and hinges of the prototype shown in Figure 6 are made of steel (approximately *210GPa* of Young modulus), the cables are made of silicone rubber and the hinges are connected to the struts. When completely assembled, the structure was weighted and the total weight was divided by the number of bars. The cables are assumed to be massless and the struts to concentrate *0.01kg/bar* approximately.

Silicone was selected to be the material of the tendons because of its great elastic range and low Young modulus, so the structure can be put under large deformations with a small load without failing. An experiment was executed to estimate the tendon's Young modulus: four *0.34m* long and *1mm* diameter rubbers were pulled and the force was acquired every *10mm* displacement by a hook scale (Table 4). The stress strain curve of this material is not linear, therefore it is convenient to focus on the range that matches the displacements of the prototype, which never exceed *20%*, leading to *19.9MPa* of Young modulus within the 7 first data points (Figure 30).

Table 4. Silicone experiment.

ΔL [m]	F [kgf]	E	σ [MPa]
0.00	0.00	0.00	0.00
0.01	0.08	0.03	0.39
0.02	0.15	0.06	1.46
0.03	0.20	0.09	1.95
0.04	0.27	0.12	2.63
0.05	0.32	0.15	3.12
0.06	0.37	0.18	3.61
0.07	0.40	0.21	3.90
0.08	0.44	0.24	4.39
0.09	0.46	0.26	4.49
0.10	0.50	0.29	4.98

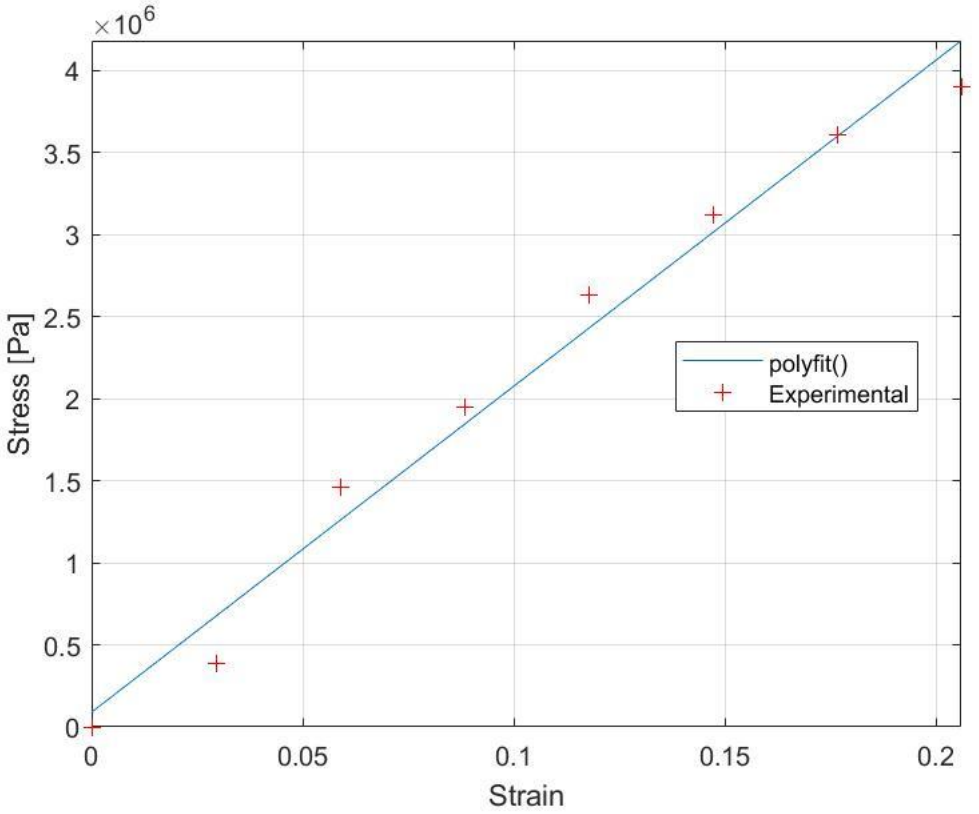

Figure 30. Stress strain curve.

5.4 Force density's relevance

The importance of the pre-stresses in chapter 3 becomes clear when looking at the results, but, in this chapter, the tension is created by external loads on the system, so the reader might question the relevance of the force density to the global stiffness in this case (equation (17)). A simple way to investigate the contribution of this force density term is by analysing the stiffness of a horizontal member (Figure 31).

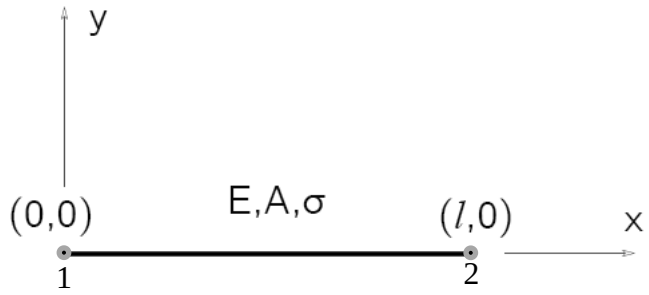

Figure 31. Horizontal element.

Following the methodology previously described, from equations (11) to (18), the members matrix M (equation (32)), S_1 (equation (33)) and the global stiffness K_G (equation (34)) may be calculated.

$$M = NC^T = \begin{bmatrix} 0 & l \\ 0 & 0 \end{bmatrix} \begin{bmatrix} -1 \\ 1 \end{bmatrix} = \begin{bmatrix} l \\ 0 \end{bmatrix} \tag{32}$$

$$S_1 = s_1 \left(I - \frac{\begin{bmatrix} l \\ 0 \end{bmatrix} [l \quad 0]}{l^2} \right) + K_B \frac{\begin{bmatrix} l \\ 0 \end{bmatrix} [l \quad 0]}{l^2} = \begin{bmatrix} K_B & 0 \\ 0 & s_1 \end{bmatrix} = \begin{bmatrix} K_B & 0 \\ 0 & s_1 \end{bmatrix} = \begin{bmatrix} \frac{EA}{l} & 0 \\ 0 & \frac{\sigma A}{l} \end{bmatrix} \tag{33}$$

$$K_G = \left([-1 \quad 1] \begin{bmatrix} -1 \\ 1 \end{bmatrix} \right) \otimes S_1 = \begin{bmatrix} S_1 & -S_1 \\ -S_1 & S_1 \end{bmatrix} = \begin{bmatrix} K_B & 0 & -K_B & 0 \\ 0 & s_1 & 0 & -s_1 \\ -K_B & 0 & K_B & 0 \\ 0 & -s_1 & 0 & s_1 \end{bmatrix} \tag{34}$$

As both s_1 and K_B terms appear in the stiffness matrix, s_1's contribution may be appraised by comparing it with K_B. However, s_1 changes depending on the tension σ, so the relevance of the force density needs to be assessed while in the range of tension experimented in this chapter (Figure 32), which does not exceed $4MPa$. Once s_1 may reach up to 16% of K_B, given the conditions of the experiments in this chapter, the possibility of neglecting the force density is finally denied.

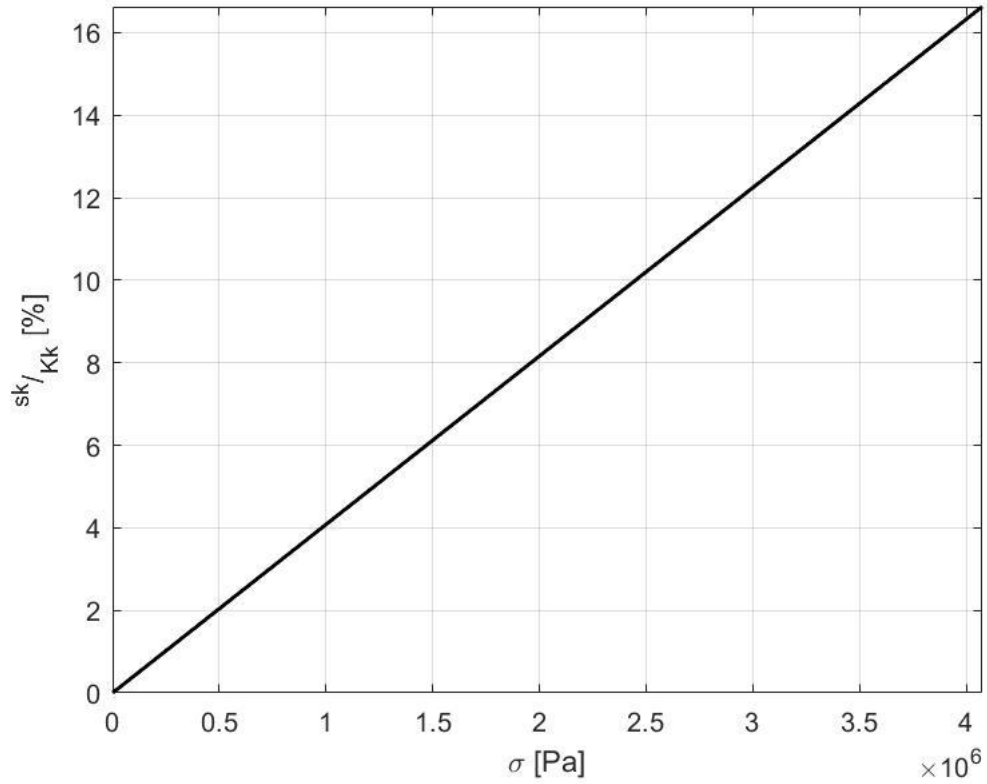

Figure 32. Relevance of s_k.

5.5 Static results and comments

A grid behind the prototype permits an accurate acquisition of the displacements. The loads to which the prototype is subjected are *0, 0.03, 0.044, 0.052, 0.061* and *0.066 kgf* (Figure 33). The prototype's behavior is represented by dashed black lines with circles representing the *10 mm* tolerance on the nodes positions, the thick red lines are the struts, the solid black lines are the cables and the thin blue lines show the natural position of the tensegrity.

In the first solution, the highlight is the behavior of the structure when subjected to self-weight only, without any loads on the cable. Each level sustains the weight of the upper ones, so the lower levels are stretched more than the others. The other five solutions follow the expected pattern: greater loads leading to greater displacements.

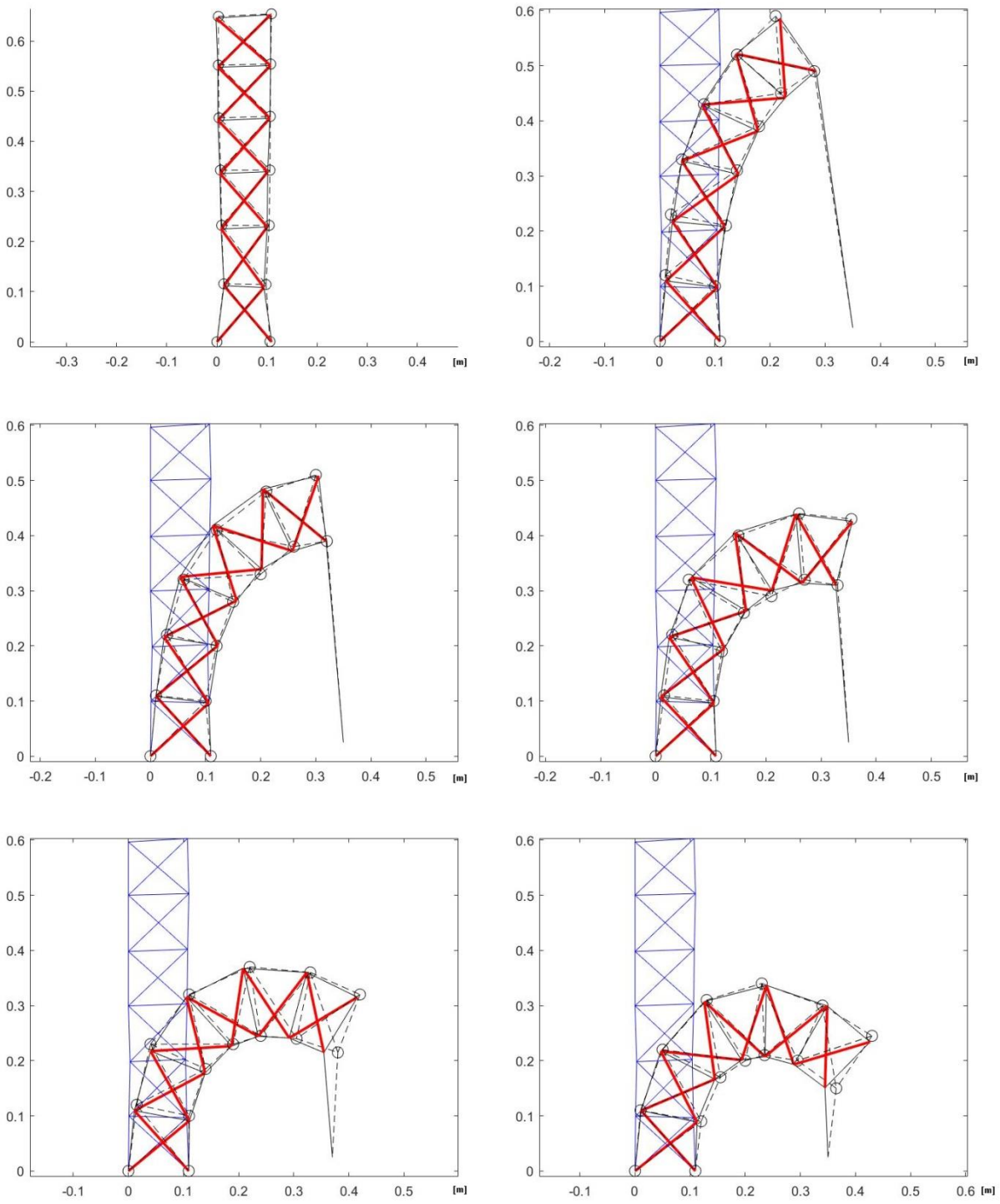

Figure 33. Validation.

5.5 Natural frequencies and comments

The 8 first natural frequencies were extracted for 200 deformed positions, the loads responsible for these displacements are indicated as a function of the total weight of the structure (Figure 34).

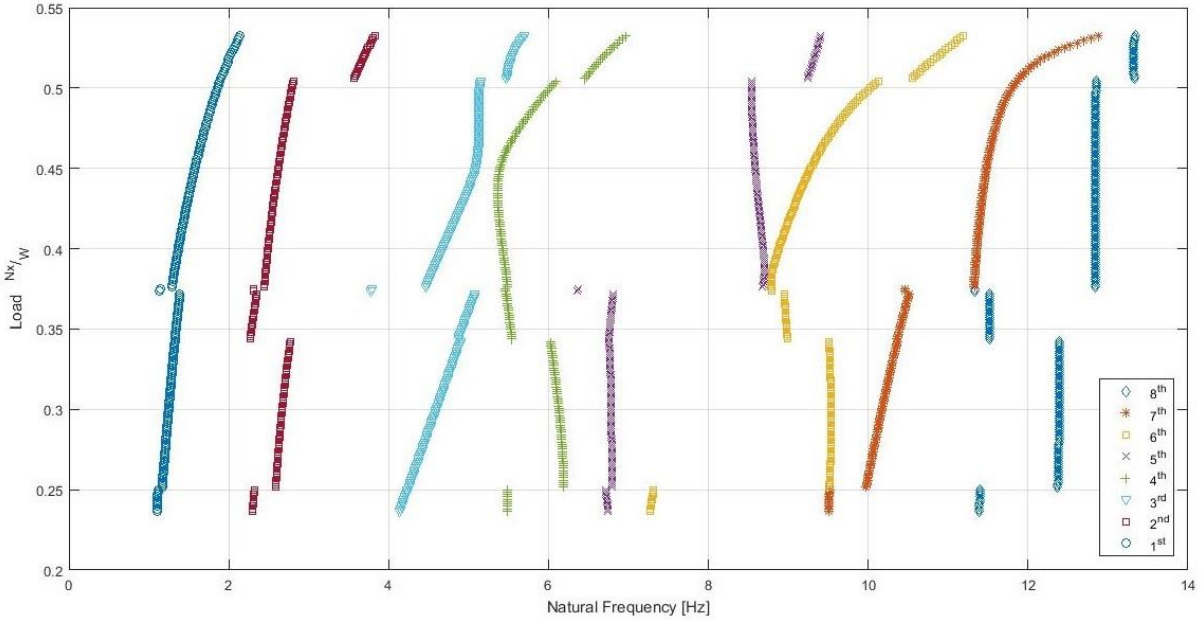

Figure 34. Natural frequencies for all deformed positions.

In most modes, the natural frequency increases with a higher load, as expected. In this analysis, slack cables were simply removed from the mesh, so there is an abrupt reduction in the stiffness matrix every time a cable becomes slack. Analogously, whenever a slack cable becomes taut, there is a sudden increment in K_G. These abrupt changes in stiffness cause the shifts in natural frequencies in Figure 34. These discontinuities can be avoided by initially pre-stressing the cables so they do not become slack during the analysis, this procedure will be incorporated in a future work.

Furthermore, the state of a certain cable may not affect all modes of vibration. For example, when the load reached approximately 25% of the weight of the structure, there was an increment in stiffness because all modes (except the third) shifted to a higher natural frequency. This means that a previously slack cable is under traction now, but the degrees of

freedom to which it is responsible do not affect the shape of the third mode of vibration considerably.

5.6 Conclusions

In this chapter, Skelton's (2009) methodology for calculating the stiffness of a pre-stressed tensegrity was combined with Euler's (incremental loads) method for solving nonlinear static analyses. This combination of methods was verified with a lightweight and flexible 2D tensegrity tower subjected to large deformations. The loads were applied through a pulling cable attached to the tip of the tower and the self-weight of the structure was considered.

A parallel experiment was executed to define the stress strain curve of the cable, which was found to be nonlinear in the elastic range. This nonlinearity is increased when the cable is greatly deformed, which explains why some experimental points do not match perfectly with simulations in the last two graphs of Figure 33. However, the vast majority of the results stayed within the tolerance, enhancing the reliability of the method.

The modal analysis for all static positions confirmed the conclusions of the previous chapter and highlighted an issue related to cables switching between slack and taut states. The future steps include avoiding this issue by pre-stressing the cables (before performing the static analysis) to postpone the occurrence of slack cables (KAN, PENG and CHEN, 2018).

Other possible extensions are the development of a vibration control strategy, driving the displacements with the tower's own tendons instead of an external pulling cable or modeling a three dimensional tower.

6 CONCLUSIONS

Tensegrity systems offer many advantages over traditional structures, such as controllable stiffness and deployable geometry, this work aimed to analyse each characteristic separately. For that, three experiments about tensegrities were executed, the first one focused on showing the relation between pre-stress and stiffness, the second involved large deformations and the third highlighted the expansion process of a deployable tensegrity.

Firstly, a four struts tensegrity prism was suggested to replace the solid cones used nowadays to support reflector antennas on satellites. This structure would be sent to space in its compact configuration to save volume and to bear the loads more easily, its expansion would happen only when in orbit following the characteristics studied in chapter 5. After completely expanded, the designer can control its stiffness as in the first prototype, so the final structure would be lighter (not only by nature, but because the loads during launch are endured in the compact shape), stiffer (or not, according to the designer's will) and would save volume in rocket. Although not a problem in space, the forces required to lift this system on Earth was also assessed in case other applications appear.

Secondly, a three struts tensegrity prism was built with metallic bars and nylon tendons, each bar had a screw to which the tendon was attached so the designer could apply torque to increase or decrease the tension in the tendons. This change in tension leads to a change in stiffness, which was assessed through modal analysis. As expected, the natural frequencies increased with the tension, confirming that the structure becomes stiffer with greater pre-stresses. A numerical model was implemented and validated with the results of the prototype.

Secondly, a four struts tensegrity prism was suggested to replace the solid cones used nowadays to support reflector antennas on satellites. This structure would be sent to space in its compact configuration to save volume and to bear the loads more easily, its expansion would happen only when in orbit following the characteristics studied in chapter 5. After completely expanded, the designer can control its stiffness as in the first prototype, so the final structure would be lighter (not only by nature, but because the loads during launch are endured in the compact shape), stiffer (or not, according to the designer's will) and would

save volume in rocket. Although not a problem in space, the forces required to lift this system on Earth was also assessed in case other applications appear.

Finally, a bi-dimensional class 2 tensegrity tower with 6 storeys was built with metallic bars and elastic cables and put under large deformations. The methodology used to calculate the stiffness of the first prototype is accurate for small displacements only, so it was combined with Euler's method for nonlinear static analysis to simulate the condition of this second prototype. The contribution to the field of this second experiment lies in the methodology, therefore its conclusion showing a good match between numerical and experimental results is the chapter's highlight.

With these three models, this work can be an initial guide to calculating tensegrity structures and mechanisms, from its kinematics and dynamics to its structural behaviour after applying either small or large loads and varying pre-tension. This last chapter involved a practical application for a tensegrity mechanism, but after completely expanded, the stiffness could be controlled as seen in chapter 3 so the natural frequency would shift from a certain excitation, or a static analysis could predict the new shape of the structure if external loads were applied, as in chapter 4.

A critical limitation of this work lies in the quality of the prototypes, especially regarding the materials properties, which were hard to approximate. A better estimative of the properties and more symmetric prototypes would have brought a better indication of the methods' accuracy. Finally, a limitation of the methodology for nonlinear analysis is the low efficiency of Euler's method, which requires a high number of steps to reach an accurate result and may be inconvenient for a model with too many elements. Nevertheless, the actual prototypes satisfied the purposes of validating the methodologies.

Tensegrities pay the price for being highly mass efficient with a slightly lower stiffness, which makes them more sensitive to vibrations. Vibration control was not appraised in this study, what comes closest is the first model with variable natural frequencies, but a more complex study with excitations and real time control would suit the future steps neatly, adding a significant argument in favour of these innovative structures.

The future steps regarding the reflector antenna improvements could be focused on the reflector surface, studying its replacement by a membrane and therefore reducing the total mass of the system. A tensegrity-membrane model would have to be defined and the behaviour of the membrane itself characterised. Furthermore, an addition to the tensegrity tower study could involve the development of a vibration control strategy, pre-stressing the

tendons to postpone the occurrence of slack cables or modeling a three dimensional tower by stacking several 4 struts mechanisms on top of each other. This combination would generate a class 2 tensegrity tower mechanism capable of transforming its shape without the action of an external pulling cable.

One aspect that keeps tensegrities from being largely used is lack of acceptance as they are recent when compared to trusses or beams. However, as the advantages are numerous and useful, it becomes a matter of establishing the reliability of the term tensegrity to make them be better availed in the future, and documenting experiments is a key step to bring this future closer.

References

ADAM, B.; SMITH, I. Active tensegrity: a control framework for an adaptive civil-engineering structure. **Computers & structures**, v. 86, n. 24, p. 2215-2223, 2008.

ARSENAULT, M.; GOSSELIN, C. M. Kinematic and static analysis of a 3-PUPS spatial tensegrity mechanism. **Mechanism and machine theory**, n. 44, p. 162-179, 2009.

ASHWEAR, N.; ERIKSSON, A. Natural frequencies describe the pre-stress in tensegrity structures. **Computers & structures**, v. 136, p. 162-171, 2014.

BALTAXE-ADMONY, L. B. et al. **Simulating the human shoulder through active tensegrity structures**. International design engineering technical conferences & computers and information engineering conference. Charlotte: ASME. 2016. p. 6.

BEL HADJ ALI, N.; RHODE-BARBARIGOS, L.; SMITH, I. F. C. Analysis of clustered tensegrity structures using a modified dynamic relaxation algorithm. **International journal of solids and structures**, n. 48, p. 637-647, 2011.

BEL HADJ ALI, N.; SMITH, I. F. C. Dynamic behavior and vibration control of a tensegriy structure. **International journal of solids and structures**, Lausanne, n. 47, p. 1285-1296, January 2010.

CAI, J. et al. Effect of initial imperfections of struts on the mechanical behaviour of tensegrity structures. **Composite structures**, v. 207, p. 871-876, January 2019.

COOK, R. D. **Finite element modeling for stress analysis**. New York: John Siley & Sons, 1995.

CRISFIELD, M. A. **Non-linear finite element analysis of solids and structures**. Chinchester: John Wiley & Sons, v. 1, 2000.

DALILSAFAEI, S.; ERIKSSON, A.; TIBERT, G. Improving bending stiffness of tensegrity booms. **International journal of space structures**, v. 27, n. 2, p. 117-129, 2012.

DJOUADI, S. et al. Active control of tensegrity systems. **Journal of aerospace engineering**, v. 11, n. 2, p. 37-44, 1998.

DOUGHTY, S. **Mechanics of machines**. New York: John Wiley & Sons, 1988.

FAZLI, N.; ABEDIAN, A. Design of tensegrity structures for supporting deployable mesh antennas. **Scientia iranica**, Tehran, n. 18, p. 1078-1087, June 2011.

FENG, X.; MIAH, M.; OU, Y. Dynamic behavior and vibration mitigation of a spatial tensegrity beam. **Engineering structures**, v. 171, p. 1007-1016, February 2018.

FRANTSEVICH, L.; GORB, S. Arcus as a tensegrity structure in the arolium of wasps (Hymenoptera: Vespidae). **Zoology**, v. 105, n. 3, p. 225-237, 2002.

FRIESEN, J. et al. **The second generation prototype of a duct climbing tensegrity robot, DuCTTv2**. 2016 IEEE International conference on robotics and automation (ICRA). Stockholm: [s.n.]. 2016. p. 2123-2128.

FULLER, B.; APPLEWHITE, E. **Synergetics:** explorations in the geometry of thinking. [S.l.]: Macmillan, 1975.

FURUYA, H. Concept of deployable tensegrity structures in space application. **International journal of space structures**, Nagoya, v. 7, n. 2, p. 143-151, May 1992.

GILEWSKI, W.; KLOSOWSKA, J.; OBARA, P. Applications of tensegrity structures in civil engineering. **Procedia engineering**, v. 111, p. 242-248, 2015.

HIBBELER, R. C. **Engineering Mechanics Statics**. 10. ed. New Jersey: Pearson Education, 2004.

HOLLAND, D.; VIRGIN, L.; PLAUT, R. Large deflections and vibration of a tappered cantilever pulled at its tip by a cable. **Journal of sound and vibration**, Durham, v. 310, n. 1-2, p. 433-441, February 2008.

HORN, R. A.; JOHNSON, C. R. **Topics in Matrix Analysis**. Cambridge: Cambridge University Press, 1994.

INGBER, D. Tensegrity: the architectural basis of cellular mechanotransduction. **Annual review of physiology**, v. 59, n. 1, p. 575-599, 1997.

JAUREGUI, V. G. **Controversial origins of tensegrity**. Symposium of the International Association for Shell and Spatial Structures. Valencia: Editorial Universitariat Politecnica de Valencia. 2009. p. 11.

JENSEN, O. et al. Finite element analysis of tensegrity structures in offshore aquaculture installations. **Aquacultural engineering**, v. 36, n. 3, p. 272-284, 2007.

JUNG, E. et al. **Design and selection of muscle excitation patterns for modeling a lower extremity joint inspired tensegrity**. IEEE International conference on robotic computing. Naples: [s.n.]. 2019. p. 282-287.

KAN, Z.; PENG, H.; CHEN, B. Complementarity framework for nonlinear analysis of tensegrity structure with slack cables. **AIAA Journal**, Dalian, v. 56, n. 12, p. 5013-5027, October 2018. ISSN 0001-1452.

KEBICHE, K.; KAZI-AOUAL, M.; MOTRO, R. Geometrical non-linear analysis of tensegrity systems. **Engineering structures**, v. 21, p. 864-876, 1999.

KURKA, P. et al. Vibration of a long, tip pulled deflected beam. **AIAA Journal**, v. 52, n. 7, p. 1559-1563, July 2014.

KURKA, P. et al. Large deflections and vibrations of a tip pulled beam with variable transversal section. **Mechanical systems and signal processing**, Campinas, v. 79, p. 271-288, October 2016.

KURKA, P. et al. **Dynamic behavior and vibration analysis of tensegrity-membrane structures**. International conference on noise and vibration engineering & international conference on uncertainty in structural dynamics. Heverlee: KU Leuven. 2018. p. 3271-3285.

LESSARD, S. et al. **A bio-inspired tensegrity manipulator with multi-DOF, structurally compliant joints**. International conference on intelligent robots and systems. Daejon: IEEE. 2016. p. 6.

LEVIN, S. The tensegrity-truss as a model for spine mechanics: biotensegrity. **Journal of mechanics in medicine and biology**, v. 2, n. 3, p. 375-388, October 2002.

MOORED, K.; BART-SMITH, H. The analysis of tensegrity structures for the design of a morphing wing. **Journal of applied mechanics**, Charlottesville, v. 74, n. 4, p. 668-676, 2007.

MOORED, K.; BART-SMITH, H. Investigation of clustered actuation in tensegrity structures. **International journal of solids and structures**, v. 46, n. 17, p. 3272-3281, May 2009.

MORTEROLLE, S. et al. Modal behaviour of a new large reflector conceptual design. **Aerospace science and technology**, Lyon, n. 42, p. 74-79, January 2015.

MOTRO, R.; NAJARI, S.; JOUANNA, P. **Static and dynamic analysis of tensegrity systems**. ASCE International symposium on shells and spatial structures. New York: Springer. 1986. p. 270-279.

MURAKAMI, H. Static and dynamic analyses of tensegrity structures. Part 1. Nonlinear equations of motion. **International journal of solids and structures**, v. 38, p. 3599-3613, 2001.

PAGITZ, M.; TUR, J. M. Finite element based form-finding algorithm for tensegrity structures. **International journal of solids and structures**, v. 46, n. 17, p. 3235-3240, 2009.

PAIVA, V.; KURKA, P.; IZUKA, J. **Kinematics and dynamics of a tensegrity structure in expansion**. 31st Congress of the international council of the aeronautical sciences. Belo Horizonte: ICAS. 2018. p. 10.

PAUL, C.; VALERO-CUEVAS, F.; LIPSON, H. Design and control of tensegrity robots for locomotion. **IEEE Transactions on robotics**, Piscataway, v. 22, n. 5, p. 944-957, October 2006. ISSN 1552-3098.

PELLEGRINO, S. **Deployable structures**. New York: Springer-Verlag Wien, 2001.

PUGH, A. **An introduction to tensegrity**. Berkeley: University of California press, 1976.

RHODE-BARBARIGOS, L. et al. Designing tensegrity modules for pedestrian bridges. **Engineering Structures**, n. 32, p. 1158-1167, January 2010.

RHODE-BARBARIGOS, L. et al. Mechanism-based approach for the deployment of a tensegrity-ring module. **Journal of structural engineering**, n. 138, p. 539-548, April 2012.

RUSSEL, C.; TIBERT, G. Deployment simulations of inflatable tensegrity structures. **International journal of space structures**, Stockholm, v. 23, n. 2, p. 63-77, June 2008.

SCHENK, M.; HERDER, J. L.; GUEST, S. D. **Design of a statically balanced tensegrity mechanism**. International design engineering technical conferences & computers and information in engineering conference. Philadelphia: ASME. 2006. p. 11.

SKELTON, R. et al. **An introduction to the mechanics of tensegrity structures**. Proceedings of the 40th IEEE conference on decision and control (Cat. No. 01CH37228). Orlando: [s.n.]. 2001. p. 4254-4259.

SKELTON, R.; DE OLIVEIRA, M. **Tensegrity systems**. New York: Springer, 2009.

SULTAN, C. Tensegrity deployment using infinitesimal mechanisms. **International journal of solids and structures**, Blacksburg, n. 51, p. 3653-3668, July 2014.

SUNNY, M.; SULTAN, C.; KAPANIA, R. Optimal energy harvesting from a membrane attached to a tensegrity structure. **AIAA Journal**, v. 52, n. 2, p. 307-319, February 2014.

SUNSPIRAL, V.; AGOGINO, A.; ATKINSON, D. **Super ball bot - structures for planetary landing and exploration for the NASA innovative advanced concepts (NIAC) program**. National Aeronautics and Space Administration NASA. [S.l.], p. 115. 2015.

TEIXEIRA, L. et al. **A numerical analysis of the dynamics of a tensegrity-membrane structure**. 31st Congress of the international council of the aeronautical sciences. Belo Horizonte: [s.n.]. 2018. p. 9.

THOMSOM, M. **The Astromesh deployable reflector**. IEEE Antennas and propagation society international symposium. 1999 Held in conjunction with: USNC/URSI National radio science meeting (Cat. No. 99CH37010). Carpinteria: [s.n.]. 1999. p. 1516-1519.

TIBERT, G. **Deployable tensegrity structures for space applications**. [S.l.]: 2002. 244p. Thesis (PhD.) - Royal Institue of Technology, Stockholm., 2002.

TRAN, H. C.; LEE, J. Geometric and material nonlinear analysis of tensegrity structures. **Acta Mechanica Sinica**, Seoul, v. 27, n. 6, p. 938–949, July 2011. ISSN 1614-3116.

WANG, N. et al. **Mechanical behavior in living cells consistent with the tensegrity model**. Proceedings of the national academy of sciences. Cambridge: [s.n.]. 2001. p. 7765-7770.

YANG, S.; SULTAN, C. Control-oriented modeling and deployment of tensegrity-membrane systems. **International journal of robust and nonlinear control**, Blacksburg, October 2016.

YANG, S.; SULTAN, C. Deployment of foldable tensegrity-membrane systems via transition between tensegrity configurations and tensegrity-membrane configurations. **International journal of solids and structures**, v. 160, p. 103-119, 2019.

ZHANG, J. Y.; OHSAKI, M. **Tensegrity structures form, stability and symmetry**. 1st. ed. Tokyo: Springer, v. 6, 2015.

ZHANG, J.; OHSAKI, M. Adaptive force density method for form-finding problem of tensegrity structures. **Internatonal journal of solids and structures**, v. 43, p. 5658-5673, 2006.

ZHANG, L.-Y. et al. A numerical method for simulating nonlinear mechanical responses of tensegrity structures under large deformations. **Journal of applied mechanics**, Beijing, v. 80, p. 061018/1-061018/10, November 2013.

ZHANG, R. et al. Theoretical analysis and experiments of a space deployable truss structure. **Composite structures**, Harbin, n. 112, p. 226-230, February 2014.

ZOLESI, V. S. et al. **On an innovative deployment concept for large space structures**. 42nd International conference on environmental systems. San Diego: AIAA American institute of aeronautics and astronautics. 2012. p. 14.

ASSOCIAÇÃO BRASILEIRA DE NORMAS TÉCNICAS. **NBR 6023**: informação e documentação: elaboração. Rio de Janeiro, 2002. 24p.

Appendix A – First modes and natural frequencies

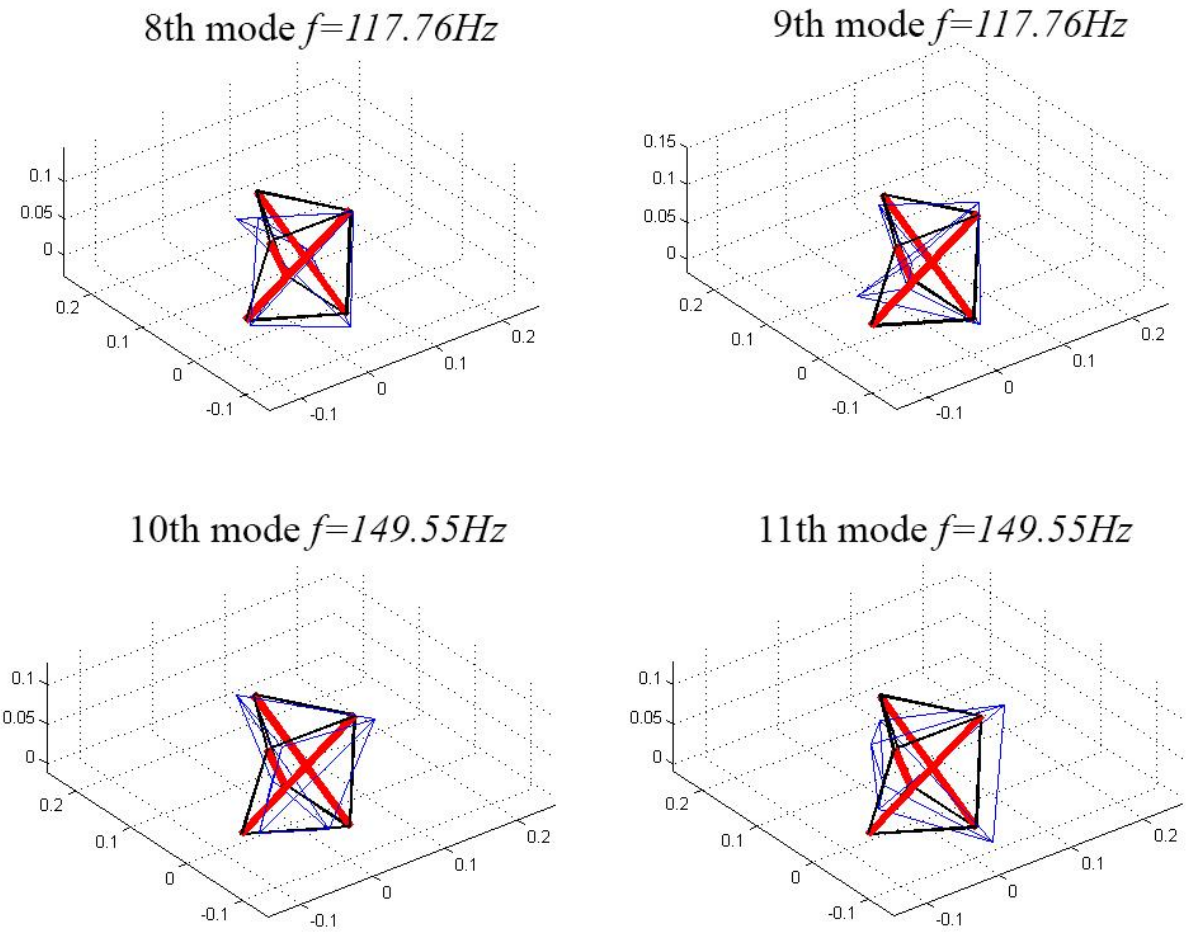

Figure 35. $\tau_H = 0$.

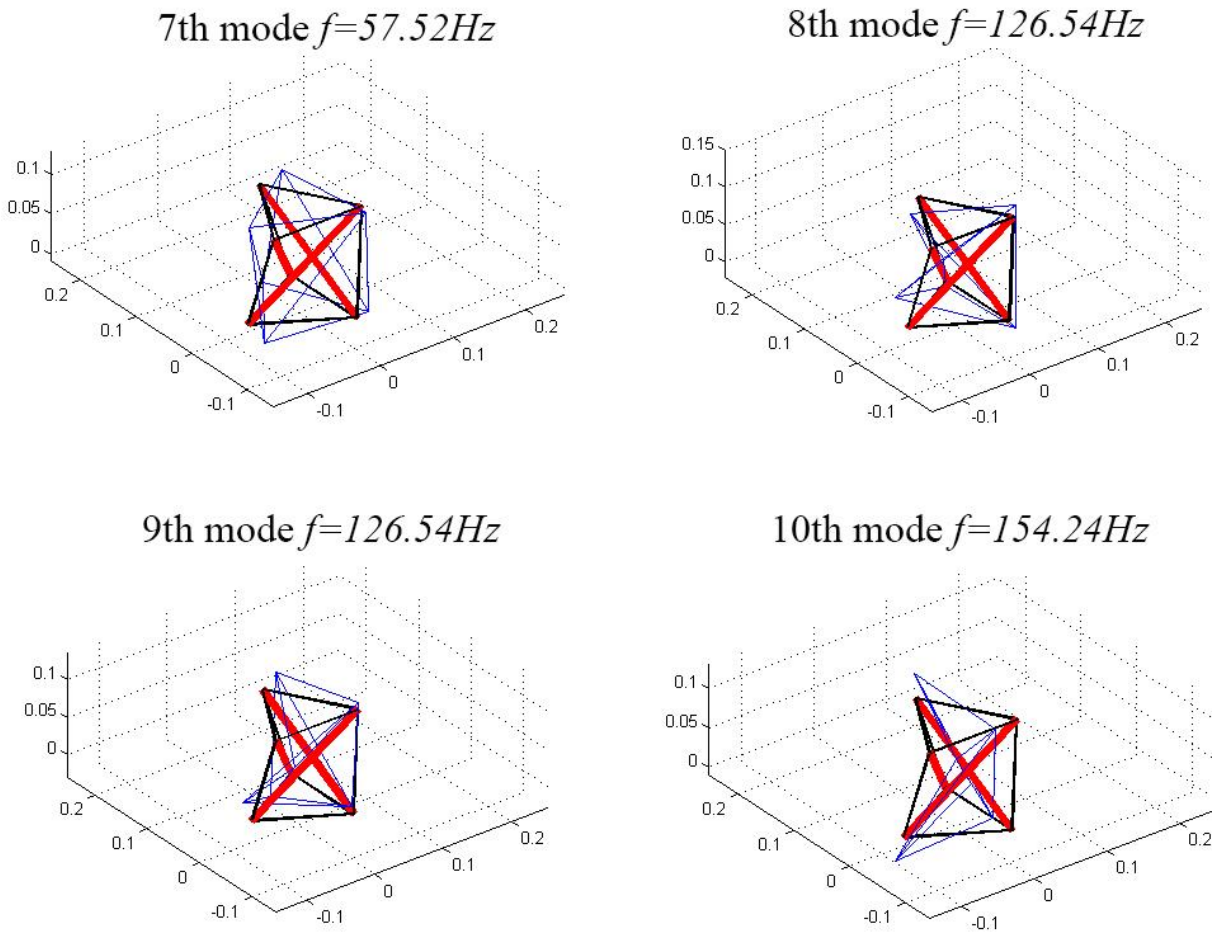

Figure 36. τ_H =10N.

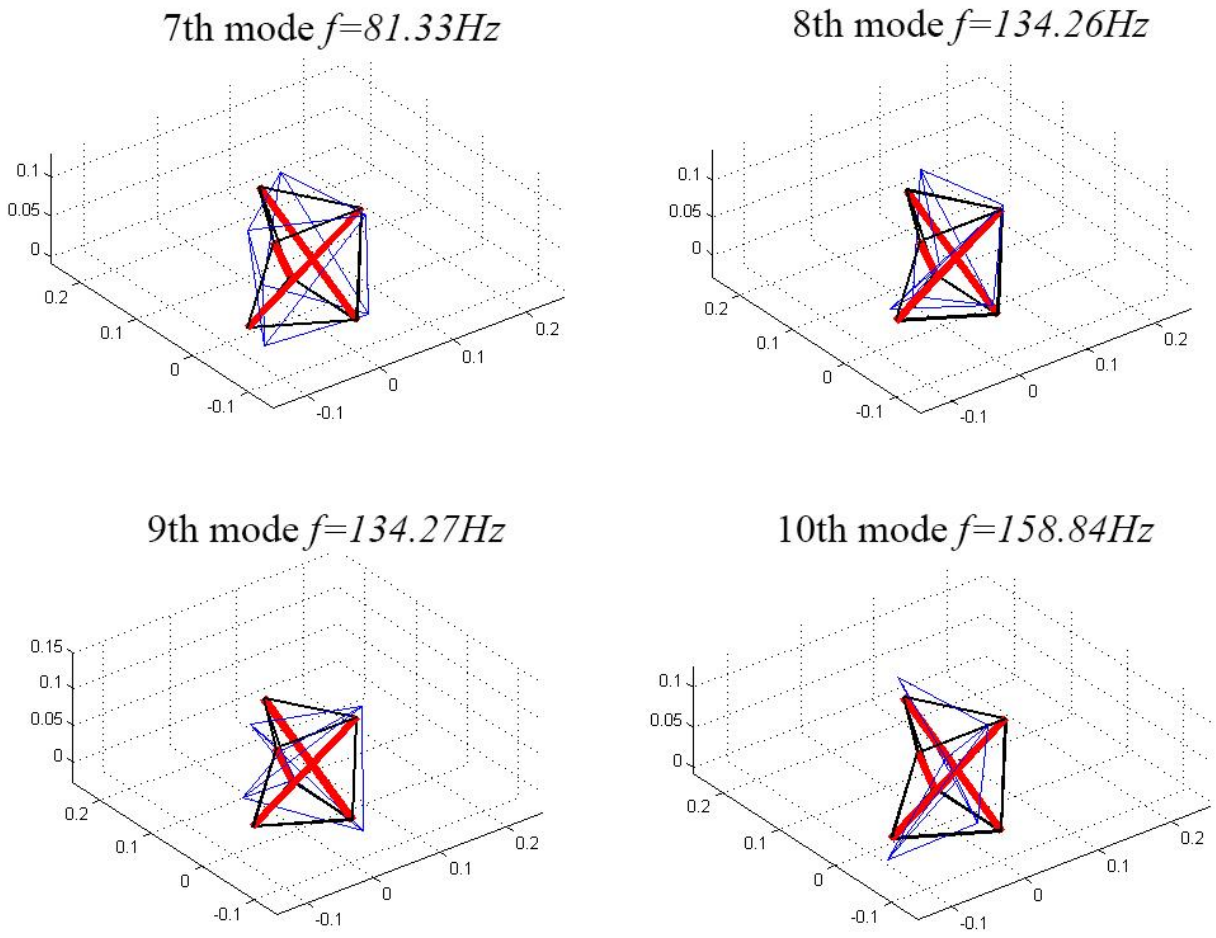

Figure 37. τ_H =20Hz.

Appendix B – Kronecker product

If H is a i x j matrix and G is a α x β matrix, the Kronecker product (HORN and JOHNSON, 1994) $H \otimes G$ of dimensions $i\alpha$ x $j\beta$ is defined in equation (35):

$$H \otimes G = \begin{bmatrix} H_{11}G & H_{12}G & \cdots & H_{1j}G \\ H_{21}G & H_{22}G & \cdots & H_{2j}G \\ \vdots & \vdots & \ddots & \vdots \\ H_{i1}G & H_{i2}G & \cdots & H_{ij}G \end{bmatrix} \rightarrow$$

$$\rightarrow H \otimes G = \begin{bmatrix} \begin{bmatrix} H_{11}G_{11} & H_{11}G_{12} & \cdots & H_{11}G_{1\beta} \\ H_{11}G_{21} & H_{11}G_{22} & \cdots & H_{11}G_{2\beta} \\ \vdots & \vdots & \ddots & \vdots \\ H_{11}G_{\alpha 1} & H_{11}G_{\alpha 2} & \cdots & H_{11}G_{\alpha\beta} \end{bmatrix} & [H_{12}G] & \cdots & [H_{1j}G] \\ [H_{21}G] & [H_{22}G] & \cdots & [H_{2j}G] \\ \vdots & \vdots & \ddots & \vdots \\ [H_{i1}G] & [H_{i2}G] & \cdots & [H_{ij}G] \end{bmatrix} \quad (35)$$